Coupling Remote Sensing with a Process Model for the Simulation of Rangeland Carbon Dynamics

Yushu Xia[1,2*], Jonathan Sanderman[1], Jennifer D. Watts[1,3], Megan B. Machmuller[4], Andrew L. Mullen[1], Charlotte Rivard[1,5†], Arthur Endsley[6], Haydee Hernandez[1,7†], John Kimball[6], Stephanie A. Ewing[3], Marcy Litvak[8], Tomer Duman[8], Praveena Krishnan[9], Tilden Meyers[9], Nathaniel A. Brunsell[10], Binayak Mohanty[11], Heping Liu[12], Zhongming Gao[12,13†], Jiquan Chen[14], Michael Abraha[14], Russell L. Scott[15], Gerald N. Flerchinger[16], Patrick E. Clark[16], Paul C. Stoy[17], Anam M. Khan[18], E.N. Jack Brookshire[3], Quan Zhang[19,20†], David R. Cook[21], Thomas Thienelt[22], Bhaskar Mitra[23], Marguerite Mauritz-Tozer[24], Craig E. Tweedie[24], Margaret S. Torn[25], and Dave Billesbach[26]

[1] Woodwell Climate Research Center, Falmouth, MA 02540, USA.

[2] Lamont Doherty Earth Observatory, Columbia University, Palisades, NY 10964, USA.

[3] Department of Land Resources and Environmental Sciences, Montana State University, Bozeman, MT 173120, USA.

[4] Natural Resources and Ecology Laboratory, Colorado State University, Fort Collins, CO 80523, USA.

[5] Center for Sustainable Development, The Brookings Institution, Washington, D.C. 20036, USA.

[6] WA Franke College of Forestry and Conservation, The University of Montana, Missoula, MT 59812, USA.

[7] The Nature Conservancy, Colorado Field Office, Boulder, CO 80302, USA.

[8] Department of Biology, University of New Mexico, Albuquerque, NM 87131, USA.

[9] Atmospheric Turbulence and Diffusion Division, National Oceanic and Atmospheric Administration, Oak Ridge, TN 37830, USA.

[10] Department of Geography and Atmospheric Science, University of Kansas, Lawrence KS 66045, USA.

[11] Biological and Agricultural Engineering Department, Texas A&M University, College Station, TX 77843, USA.

[12] Department of Civil and Environmental Engineering, Washington State University, Pullman, WA 99164, USA.

[13] School of Atmospheric Sciences, Sun Yat-sen University, Zhuhai 519082, China.

[14] Department of Geography, Environment, and Spatial Sciences, Michigan State University, East Lansing, MI 48823, USA.

[15] Southwest Watershed Research Center, USDA Agricultural Research Service, Tucson, AZ 85719, USA.

[16] Northwest Watershed Research Center, USDA Agricultural Research Service, Boise, ID 83702, USA.

[17] Department of Biological Systems Engineering, University of Wisconsin-Madison, Madison, WI 53706, USA.

[18] Department of Forest and Wildlife Ecology, University of Wisconsin-Madison, Madison, WI 53706, USA.

[19] School of Public and Environmental Affairs, Indiana University, Indianapolis, IN 46202, USA.

[20] State Key Laboratory of Water Resources Engineering and Management, Wuhan University, Wuhan 430072, China.

[21] Division of Environmental Science, Argonne National Laboratory, Lemont, IL 60439, USA.

[22] Department of Geoecology, Martin Luther University Halle-Wittenberg, Wittenberg 06099, Germany.

[23] Information and Computational Science, James Hutton Institute, Aberdeen AB15 8QH, United Kingdom.

[24] Department of Biological Sciences, The University of Texas at El Paso, El Paso, TX 79902, USA.

[25] Climate and Ecosystem Sciences Division, Lawrence Berkeley National Laboratory, Berkeley CA 94720, USA.

[26] Department of Biological Systems Engineering, University of Nebraska-Lincoln, Lincoln, NE 68588, USA.

* Corresponding author: Yushu Xia (yushuxia@ldeo.columbia.edu)

† Current address

Key Points:

- The Rangeland Carbon Tracking and Monitoring System was calibrated to simulate vegetation type-specific rangeland C dynamics
- Regional variability in carbon fluxes and soil organic carbon is well represented by a remote sensing-driven process modeling approach
- Soil organic carbon stocks in Western and Midwestern U.S. rangelands increased over the past 20 years due to increased precipitation

Abstract

Rangelands provide significant environmental benefits through many ecosystem services, which may include soil organic carbon (SOC) sequestration. However, quantifying SOC stocks and monitoring carbon (C) fluxes in rangelands are challenging due to the considerable spatial and temporal variability tied to rangeland C dynamics, as well as limited data availability. We developed a Rangeland Carbon Tracking and Management (RCTM) system to track long-term changes in SOC and ecosystem C fluxes by leveraging remote sensing inputs and environmental variable datasets with algorithms representing terrestrial C-cycle processes. Bayesian calibration was conducted using quality-controlled C flux datasets obtained from 61 Ameriflux and NEON flux tower sites from Western and Midwestern U.S. rangelands, to parameterize the model according to dominant vegetation classes (perennial and/or annual grass, grass-shrub mixture, and grass-tree mixture). The resulting RCTM system produced higher model accuracy for estimating annual cumulative gross primary productivity (GPP) ($R^2 > 0.6$, RMSE < 390 g C m^{-2}) than net ecosystem exchange of CO_2 (NEE) ($R^2 > 0.4$, RMSE < 180 g C m^{-2}), and captured the spatial variability of surface SOC stocks with $R^2 = 0.6$ when validated against SOC measurements across 13 NEON sites. Our RCTM simulations indicated slightly enhanced SOC stocks during the past decade, which is mainly driven by an increase in precipitation. Regression analysis identified slope, soil texture, and climate factors as the main controls on model-predicted C sequestration rate. Future efforts to refine the RCTM system will benefit from long-term network-based monitoring of rangeland vegetation biomass, C fluxes, and SOC stocks.

Plain Language Summary

Rangelands play a crucial role in providing various ecosystem services, including the potentially significant but highly uncertain benefits associated with climate mitigation through increased SOC storage. Accurate estimates of long-term C storage and changes are challenged, however, by the diversity in rangelands and limited field observations currently available. In this work, we leveraged multiple publicly available datasets, including remote sensing observations, tower-based carbon flux measurements from over 60 rangeland sites in the Western and Midwestern U.S., and other environmental datasets, to build the process-based Rangeland Carbon Tracking and Monitoring (RCTM) modeling system, for the simulation of 20 years of change in rangeland C. The regionally calibrated RCTM system performs well in estimating spatial and temporal rangeland C fluxes as well as spatial SOC storage. RCTM simulation results revealed increased SOC storage and rangeland productivity that is well represented by remote sensing signals and driven by annual precipitation patterns. Since the RCTM system developed by this work can be used to generate accurate spatial and temporal estimates of SOC storage and C fluxes at fine spatial (30 m) and temporal (every 5 days) resolutions, it will be well-suited for informing rangeland C management strategies and improving broad-scale policy making.

Abbreviations

C, carbon; DNDC, Denitrification-Decomposition; DSM, digital soil mapping; fPAR, fraction of absorbed photosynthetically active radiation; GEE, Google Earth Engine; GPP, Gross Primary Productivity; L4C, Level 4 Carbon; LOOCV, leave-one-out cross-validation; LUE, light use efficiency; MBE, mean bias error; NDVI, Normalized Difference Vegetation Index; NEE, net ecosystem exchange of carbon dioxide; NEON, National Ecological Observatory Network; NIR, near infrared band; NLCD, National Land Cover Database; NLDAS, North American Land Data Assimilation System; NPP, net primary productivity; PI, principal investigator; QC, quality

control; RAP, Rangeland Analysis Platform; RCTM, Rangeland Carbon Tracking and Management; RECO, ecosystem respiration; RMSE, Root Mean Square Error; RothC, Rothamsted Carbon; RS, remote sensing; SMAP, Soil Moisture Active-Passive; SMLR, stepwise multiple linear regression; SOC, soil organic carbon; SOM, soil organic matter; STARFM, Spatial and Temporal Adaptive Reflectance Fusion Model; VPD, vapor pressure deficit.

1 Introduction

Rangelands, which include a wide range of landscapes primarily composed of grasses, forbs, and shrubs that are often grazed or browsed by domestic livestock and/or wild animals, cover more than 30% of the land area (~ 2.7 million km^2) of the contiguous United States and have a significant global presence (54%) (Chen et al., 2015; Olson et al., 2001; Reeves & Mitchell, 2011). It has been well established that rangelands provide many crucial ecosystem services, including habitat biodiversity, forage production, water retention, nutrient cycling, and carbon (C) sequestration and storage (Maher et al., 2021; Phukubye et al., 2022; Waterhouse et al., 2023). Unfortunately, grassland conversion to cropland and improper management (e.g., overgrazing) have historically contributed to land degradation and C loss in western U.S. rangelands, which can be further exacerbated by extreme climate events such as droughts (Holechek et al., 2020). Restoring degraded rangelands and improving land management are therefore high priority conservation goals having multiple ecosystem service benefits (Wilson et al., 2008). Improved rangeland management also holds possibly significant but highly uncertain potential for climate mitigation primarily through soil organic carbon (SOC) sequestration (Derner et al., 2019; Fargione et al., 2018). The uncertainty arises from factors such as extensive rangeland sizes, limited availability of in-situ field data, and substantial spatial and temporal variability associated with drivers of SOC change (i.e., environmental and management factors) such as moisture status and temperature, vegetation composition, soil properties, and grazing timing and intensity, (Booker et al., 2013; Derner & Schuman, 2007; Hill et al., 2006). In order to facilitate accurate estimates of rangeland C benefits, it is essential to develop a data-driven framework that combines process-based representation of rangeland C dynamics with multi-source, observation-based environmental datasets.

In-situ field measurements provide crucial observations of rangeland C dynamics. Flux tower observations are often used to quantify net ecosystem exchange (NEE), which represents C fluxes between land and atmosphere that can be further partitioned into gross primary productivity (GPP) and ecosystem respiration (RECO) (Oliphant, 2012; Tramontana et al., 2020). Field sampling campaigns are essential for directly measuring SOC stocks and the associated changes (Nave et al., 2021), which complements C fluxes observed from flux towers. However, direct field measurements can be both expensive and labor-intensive to accurately capture the vast and complex rangeland landscape. Upscaling in-situ observations of C fluxes and SOC stocks, using models coupled with remote sensing (RS) and large-scale surveys-derived environmental variable datasets can estimate long-term C budgets at large geographic scales (Heuvelink et al., 2021; Krause et al., 2022; Sanderman et al., 2017; Turner et al., 2004), but approaches need to be carefully designed to maximize accuracy.

The empirical, digital soil mapping (DSM) approach has been widely used for estimating SOC stocks by taking advantage of the connection between environmental variables and soil C dynamics (Minasny & McBratney, 2015; Santra et al., 2017). However, despite its rapid and

cost-effective nature, this approach is less frequently used for estimating changes in SOC stocks or C fluxes, primarily due to the scarcity of data on changes in SOC that are needed for statistical model training and verification. In contrast to purely data-driven empirical upscaling approaches, process-based models incorporate mathematical representations of underlying system processes, such as heat transfer, hydrologic flows, and C cycling (Doblas-Rodrigo et al., 2022; Khalil et al., 2020; Yagasaki & Shirato, 2014). Consequently, they possess the capability to generate process-based outcomes (e.g., SOC stock changes) and scenario-based estimates (e.g., C fluxes under different climate and management conditions) for longer term predictions.

Process-based modeling of rangeland C fluxes and SOC stocks can be implemented using two options, namely a management-driven approach or a RS-driven approach. In the management-driven approach, activity data such as livestock numbers and grazing periods are combined with climate and soil information to simulate plant growth and soil C dynamics (Arndt et al., 2022; Smith et al., 2014; Zhang et al., 2017). Adopting this approach necessitates the collection of detailed management data, which can be extremely difficult for large-scale rangeland monitoring efforts. Even though there has been a major push to automate the collection of management data through the use of RS, tracking animal numbers and movements remains challenging (Ali et al., 2016; Lange et al., 2022; Stoy et al., 2021). Current rangeland modeling efforts used to estimate management effects on SOC typically rely on the use of default parameters and model structures, such as those used in DAYCENT (Chang et al., 2015; Parton et al., 1998), Denitrification-Decomposition (DNDC) (Li et al., 1994; Wang et al., 2022), or Rothamsted Carbon (RothC) (Coleman & Jenkinson, 1996; Jebari et al., 2021) because there is a general lack of calibration and validation data suited to represent specific management scenarios (e.g., adaptive grazing practices). Due to data limitations, their efforts cannot fully account for system variability and generate predictions at the scale that is relevant to management.

The RS-driven process-based modeling approach is particularly helpful in situations where management datasets are unavailable or scarce, because RS data can be used as a proxy for vegetation productivity and growth, due to the close association between plant biomass and RS spectral bands or multi-band indices (Numata et al., 2007; Sibanda et al., 2016; Xu et al., 2008). Moreover, RS datasets can provide more refined information regarding spatial variability, which would be difficult to capture using management datasets. Utilizing RS for rangeland monitoring assumes that RS can adequately capture management effects via changes in plant cover and productivity. However, there is significant uncertainty regarding the efficacy of RS to capture management, so ground-truth data is crucial for the parameterization and evaluation of RS-driven models for rangeland monitoring (Reinermann et al., 2020). Large datasets collected through network-based measurements, such as flux tower-based observations of C fluxes and field-based measurements of SOC stocks (Biederman et al., 2017; Chu et al., 2023; Hinckley et al., 2016), offer the best representation of rangeland C dynamics under different soil, climate, and vegetation conditions, and thus are well-suited for regional model calibration and validation.

The RS-driven modeling approach has a long legacy for use in cropping and forest systems (Wang et al., 2011; Watts et al., 2023; Zhou et al., 2021) and global scale monitoring (Endsley et al., 2020); however, to the best of our knowledge, there has not been a RS-driven regional model that is designed and parameterized specifically to evaluate decadal-scale C dynamics and track SOC changes under different vegetation types for U.S. rangelands. The objective of our work was to bridge this gap with a framework that: (1) incorporates fine-

resolution, long-term geospatial datasets that can be obtained either from publicly available data sources or through data fusion, as model inputs; (2) derives regional vegetation class-specific parameters through model calibration and validation using flux tower network datasets collected from Western and Midwestern U.S. rangelands; (3) performs model evaluation using SOC stock measurements; (4) provides estimates and visualizations of modeled rangeland C dynamics for the period from 2003 to present, and at a spatial scale relevant to land managers.

2 Materials and Methods

2.1 Overview of the Rangeland Carbon Tracking and Monitoring system

To provide a framework tracking regional rangeland C dynamics, we developed a process-based RS-driven modeling system called the Rangeland Carbon Tracking and Monitoring (RCTM) model. The RCTM system integrates RS-informed geospatial datasets and in-situ field measurements with process-based representation of the carbon cycle (SI: Table A1). The RCTM system first estimates plant productivity using RS and environmental inputs. The estimates are then fed into a soil process-based model to simulate C dynamics. There are three main components involved in the system (Fig. 1): (1) The Spatial and Temporal Adaptive Reflectance Fusion Model (STARFM) algorithm (Gao et al., 2006; Watts et al., 2011) is utilized to derive estimates of fraction of absorbed photosynthetically active radiation (fPAR) at a 30 m resolution and at five-day intervals; (2) RS or survey-derived variables, including soil properties, climate factors, and vegetation types, are utilized in conjunction with fPAR through light-use efficiency (LUE) algorithms adapted from NASA's Soil Moisture Active-Passive (SMAP) Level 4 Carbon (L4C) model (Endsley et al., 2020) to derive estimates of GPP, where vegetation type-specific parameters associated with environmental variable-based constraints on LUE are subject to model calibration; (3) Aboveground and belowground biomass are estimated from GPP using algorithms adapted from DAYCENT (Parton et al., 1998) and then allocated to different soil organic matter (SOM) pools specified within a process-based model structure adapted from the RothC model (Coleman & Jenkinson, 1996). This last step derives estimates of C fluxes and SOC stocks, with flux tower-based measurements of NEE used to parameterize factors associated with SOM decomposition.

The main inputs for RCTM include soil properties (soil texture, moisture, and temperature), climate variables (air temperature, vapor pressure deficit (VPD), solar radiation), land cover type represented by fractional coverage of different vegetation types, and RS-derived fPAR (Table 1). Model outputs include 30 m resolution estimates of rangeland productivity represented by GPP at five-day intervals, net C fluxes represented by NEE at five-day intervals, and annual surface depth SOC stocks over the 20-year record (2003 – 2022). The development and application steps for RCTM are outlined in SI: Fig. A1.

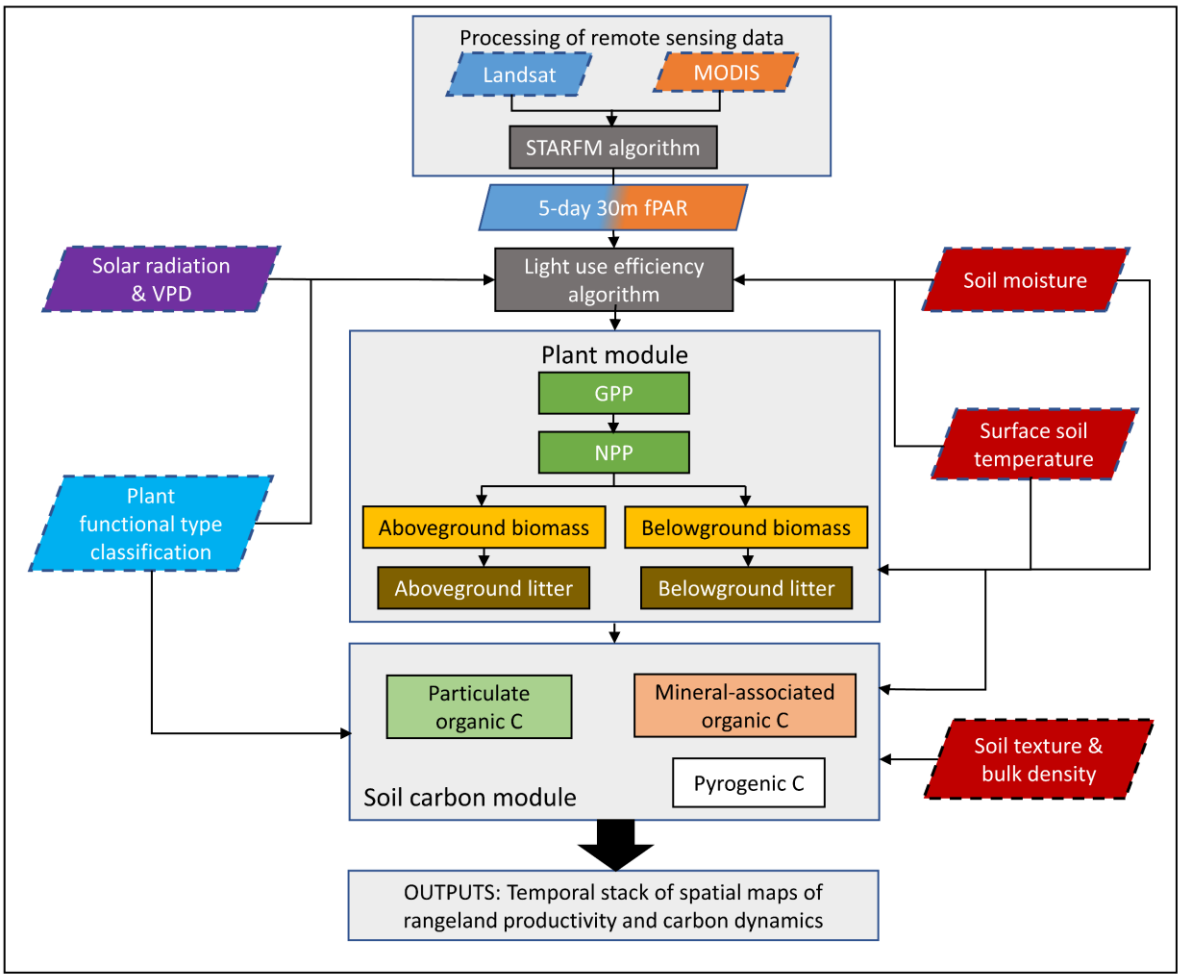

243

244 **Figure 1.** Components of Rangeland Carbon Tracking and Monitoring (RCTM) system. The
245 primary RCTM inputs include remote sensing images, soil properties, climate data, and
246 vegetation type, while the outputs include spatial and temporal estimates of rangeland carbon
247 dynamics.
248

Table 1. The input environmental datasets for the Rangeland Carbon Tracking and Monitoring (RCTM) system.

Data type	Variables [a]	Original resolution		Full temporal coverage	Usage [b]	Source and reference [c]
		Spatial	Temporal			
Soil properties	Clay%	100 m	Only once in time		Model spin-up, NEE calibration, SOC estimation, and site-based correlation analysis	SoilGrids+ (Ramcharan et al., 2018)
	Surface and root zone soil moisture	0.125°	Hourly	Since 1979	GPP calibration, model spin-up, NEE calibration, SOC estimation, and site-based correlation analysis	NLDAS (Xia et al., 2012)
	Surface soil temperature				GPP calibration, model spin-up, NEE calibration, SOC estimation, and site-based correlation analysis	
Climate	VPD	1 km	Daily	Since 1980	GPP calibration and site-based correlation analysis	DAYMET v4 (Thornton et al., 2022)
	Air temperature	1km	Daily	Since 1980	Site-based correlation analysis	
	Precipitation					
	Solar Radiation	0.125°	Hourly	Since 1979	GPP calibration	NLDAS (Xia et al., 2015)
Biotic	fPAR	500 m	Every 4 days	Since 2002	GPP calibration (coarse resolution) in SI: Appendix C	MODIS (Schaaf & Wang, 2015)
		30 m	Every 5 days	Since 2002	GPP calibration (fine resolution) and site-based correlation analysis	STARFM (Gao et al., 2006; Watts et al., 2011)
	Land cover type%	30 m	Annually	Since 1984	Vegetation type assignment	RAP (Jones et al., 2018)
Topography	Elevation	30 m	Only once in time		Site-based correlation analysis	SRTM (van Zyl, 2001)
	Slope					

[a] Clay%: soil clay content; fPAR: fraction of absorbed photosynthetically active radiation; VPD: vapor pressure deficit.
[b] GPP: gross primary productivity; NEE: net ecosystem exchange; SOC: soil organic carbon.
[c] DAYMET: Daily Surface Weather and Climatological Summaries; MODIS: Moderate Resolution Imaging Spectroradiometer; NLDAS: North American Land Data Assimilation System; RAP: Rangeland Analysis Platform; SRTM: Shuttle Radar Topography Mission.

2.2 Study sites and data sources

For model parameterization, study sites were selected from the Ameriflux (Novick et al., 2018; https://ameriflux.lbl.gov/) and National Ecological Observatory Network (NEON) networks (Keller et al., 2008; https://www.neonscience.org/) within the Western and Midwestern U.S. states (Fig. 2). We first identified all of the flux tower sites located within the region and classified as grasslands ('GRA'), savannas ('SAV'), or open shrublands ('OSH'), as well as those identified under grassland or pasture-relevant classes according to the National Land Cover Database (NLCD) data layers (Homer et al., 2007; Homer et al., 2015). We then screened the identified sites to include only those dominated by grass coverage (≥ 50%) by surveying publications associated with the flux tower datasets, examining Phenocam images (Brown et al., 2016) or online photos, and by reaching out to tower principal investigators (PIs) for confirmation. The retained 61 sites were then categorized into four different vegetation types: (1) perennial and/or annual grass; (2) managed hay and pasture; (3) grass-shrub mixture; (4) grass-tree mixture. The classification was determined using land cover information extracted from the NLCD and Rangeland Analysis Platform (RAP) (Jones et al., 2018) supplemented with literature and PI-provided site information. Sites included in class (2) differ from native grasslands in that the sites are being actively managed meaning some combination of sown grass species, irrigation, and fertilization. The coverage threshold for shrubs and trees was set at 30% for classes (3) and (4). Additional details regarding the Ameriflux and NEON sites can be found in SI: Appendix B.

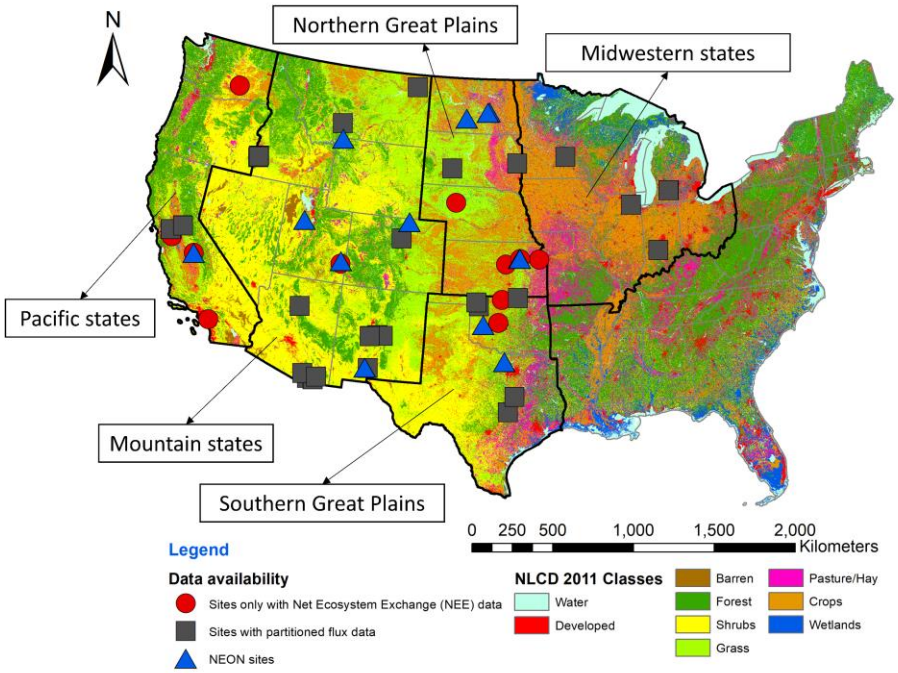

Figure 2. Ameriflux and National Ecological Observatory Network (NEON) sites selected for model calibration and validation. The sites are divided into different groups based on data availability. Different USDA agricultural regions are delineated by thick black lines, and different land use types are color-coded according to the National Land Cover Database (NLCD) dataset.

We acquired flux observations and environmental variable datasets for the retained Ameriflux and NEON sites, either from the online portal (https://ameriflux.lbl.gov/) or directly from flux tower PIs. We also documented site location, soil and vegetation type, flux tower height, data coverage, and variable availability for each site (SI: Table B1). Based on data availability, the sites were further divided into three categories (Fig. 2): (1) those that include NEE measurements only, (2) those that include both NEE and model-partitioned GPP and RECO data, and (3) those that belong to the NEON network and therefore have not only NEE and GPP/RECO data but also SOC measurements (Hinckley et al., 2016). In some cases, tower PIs expressed concerns about the quality of GPP data due to flux partitioning issues (Desai et al., 2008; Sulman et al., 2016). Consequently, we assigned these sites to the first category. Overall, we obtained data from 17, 31, and 13 sites in categories 1, 2, and 3, respectively. The flux datasets from the retained sites were quality controlled and harmonized using standard methods (Section 2.3) before being used for model calibration and validation (Sections 2.5 and 2.6).

To represent the local representativeness of the flux towers, shapefiles were created in R (R Core Team, 2023) using small (90 m × 90 m) or large (510 m × 510 m) grid sizes determined by employing a threshold value based on the flux tower height of 8 m to approximate footprints (SI: Table B1). The shapefiles were used for extraction of MODIS and Landsat RS inputs, as well as variable inputs in subsequent steps (Fig. 1).

2.3 Quality control of C flux datasets

A number of quality control (QC) measures were applied to the C flux (NEE and GPP) datasets to alleviate bias that can influence subsequent model parameterization steps. First, daily GPP and NEE results, as well as the associated meteorological measurements (e.g., air temperature, precipitation), were plotted to allow the visual identification of potential outliers or noise including: (1) extended periods with GPP reported as zero, especially during the growing season; (2) multiple GPP peaks with similar magnitudes observed during the growing season; (3) irregular spikes or sudden changes in GPP or NEE, particularly during the non-growing season. For sites with observations falling within category (1), we worked with flux tower PIs to determine whether it was necessary to replace the identified data points with no-value (NAN) flags. In the case of data points identified through category (2), we consulted with flux tower PIs to confirm whether the presence of multiple peaks could be attributed to grazing or the growth of multiple vegetation species (e.g., C3 and C4) at the sites before determining whether to retain the data points. Finally, outlier peaks identified in category (3) were removed using a moving window approach adapted from the outlier removal methods designed for time series datasets (Hartigan et al., 2019; Kelley, 2013). This involved establishing the median value of a 15-day period as a reference value, and then any observation that deviated from its reference by more than twice the standard deviation of the flux measurements at the site level was removed. The quality controlled daily GPP and NEE datasets were then classified into the four vegetation types defined in Section 2.2.

2.4 Remote sensing data extraction and processing

We derived 30 m estimates of fPAR at five-day intervals by employing the STARFM algorithm (Gao et al., 2006; Watts et al., 2011), which leverages the high temporal resolution of MODIS inputs (500 m, daily) and high spatial resolution of Landsat images (30 m, every 8

days). We first extracted MODIS images from the Nadir Bidirectional Reflectance Distribution Function Adjusted Reflectance (NBAR) product (MCD43A4 V6) (Schaaf & Wang, 2015) for the study sites, followed by the application of standard QC measures, which included the removal of cloudy pixels using the cloud bitmask and the exclusion of snow-covered pixels based on the normalized difference snow index (Hall et al., 2002). Subsequently, we calculated temporal averages at the pixel level over a 20-day moving window as a smoothed dataset, which was used to replace missing data or cropped pixels from the previous step. The Landsat images were combined from Landsat 5, 7, and 8 surface reflectance products from Collection 2 (Kovalskyy & Roy, 2013; Roy et al., 2014; Williams et al., 2006) to derive long-term records with finer 8-day temporal fidelity than the standard 16-day repeat sampling from individual Landsat satellites. QC was carried out to first exclude cloudy and snow-covered pixels using the dilated cloud, cirrus, cloud shadow, and snow bitmasks. After applying the dilated cloud bitmask, haze and thin cloud edges were often still present based on visual assessment of Landsat imagery. These cloud remnants were removed by applying an additional 15-pixel radius buffer. Images containing considerable cloud and snow contamination (>60%) were removed from the time series. To account for Landsat 7 scan-line gaps and to recover image areas that were removed from the augmented cloud masking, the masked Landsat images were spatially gap-filled using local histogram matching (USGS, 2004). First, a median composite image was generated with the nearest two months of imagery. A linear regression determined the line of best fit between pixels in the composite image and pixels in the cloud-masked image within a 50-pixel moving window. Linear regression coefficients within each moving window were applied to the composite image to fill no data pixels in the masked image. Finally, pixels containing water were removed using the water bitmask.

The extracted MODIS and Landsat scenes which overlapped on same dates were then utilized by the STARFM algorithm (Gao et al., 2006; Watts et al., 2011) to develop surface reflectance estimates at a 30 m spatial resolution and 5-day temporal frequency for individual bands. The red (RED) and near-infrared (NIR) bands were used to derive the estimates of normalized difference vegetation index (NDVI; Eq. 1) (Tucker, 1979) and scaled surface reflectance (SSR; Eq. 2). Erroneous NDVI observations were filtered by removing values where the rolling 14-day median was greater than two times the rolling 365-day standard deviation. This conservative filter mainly functioned to remove NDVI observations over snow and clouds that were missed during masking. Temporal gaps in NDVI were filled using linear interpolation.

$$\mathrm{NDVI} = \frac{\mathrm{NIR}-\mathrm{RED}}{\mathrm{NIR}+\mathrm{RED}} \quad \text{(Eq. 1)}$$

$$\mathrm{SSR} = \frac{1+\mathrm{NDVI}}{1-\mathrm{NDVI}} \quad \text{(Eq. 2)}$$

Finally, fPAR was calculated using Eq. 3-5, with the minimum and maximum NDVI and SSR reference thresholds corresponding to the 2nd and 98th percentiles of the time series values for all retained Ameriflux sites. The minimum and maximum fPAR reference values were determined through Monte-Carlo analysis for each vegetation type. Specifically, potential reference values were randomly sampled from a uniform distribution and used to predict GPP. The predicted GPP was then compared with the observed GPP (see Section 2.5), and the optimal combination of values that resulted in the best-fitted vegetation type-specific model were determined as fPAR reference values.

$$\mathrm{fPAR}_{\mathrm{NDVI}} = \frac{(\mathrm{NDVI}-\mathrm{NDVI}_{\mathrm{min}})\times(\mathrm{fPAR}_{\mathrm{max}}-\mathrm{fPAR}_{\mathrm{min}})}{(\mathrm{NDVI}_{\mathrm{max}}-\mathrm{NDVI}_{\mathrm{min}})} \quad \text{(Eq. 3)}$$

$$\mathrm{fPAR_{SSR}} = \frac{(\mathrm{SSR}-\mathrm{SSR_{min}})\times(\mathrm{fPAR_{max}}-\mathrm{fPAR_{min}})}{(\mathrm{SSR_{max}}-\mathrm{SSR_{min}})} \quad \text{(Eq. 4)}$$

$$\mathrm{fPAR} = \frac{\mathrm{fPAR_{NDVI}} + \mathrm{fPAR_{SSR}}}{2} \quad \text{(Eq. 5)}$$

The extraction and QC processing of both MODIS and Landsat data were implemented within the Google Earth Engine (GEE) platform (Gorelick et al., 2017), while the implementation of the STARFM algorithm and the following RS data processing steps were realized using Python (Rossum & Drake, 1995). All the codes used in this and subsequent sections are openly available via Github: https://github.com/xiayushu/RCTM-soil-carbon.

2.5 GPP model estimation and calibration

The LUE algorithms used for the GPP calculation were adapted from the SMAP's L4C model (Endsley et al., 2020). In RCTM, the estimation of actual LUE is based on scaling the potential maximum LUE by modifiers including root zone (ca. 60 cm depth) soil moisture, surface 5 cm soil temperature, and VPD (SI: Fig. A2), where threshold values for these modifiers were established for both upper and lower bound values. The GPP is calculated based on estimated LUE, STARFM-derived fPAR detailed in Section 2.4, and shortwave incoming solar radiation (SW_IN) using Eq. 6.

$$\mathrm{GPP} = \mathrm{LUE} \times \mathrm{SW\_IN} \times 0.45 \times \mathrm{fPAR} \quad \text{(Eq. 6)}$$

Where GPP represents gross primary productivity (g C m^{-2}), LUE represents light use efficiency (g C MJ^{-1}) estimated based on maximum LUE adjusted by environmental modifiers, SW_IN represents shortwave incoming solar radiation (MJ m^{-2}), fPAR represents fraction of absorbed photosynthetically active radiation, and 0.45 reflects the well-established observation that about 45% of incoming shortwave radiation is in photosynthetically active wavelengths (He et al., 2022).

To facilitate GPP calibration, we extracted root zone soil moisture, soil temperature at 5 cm surface depth, SW_IN from NLDAS (Xia et al., 2012), and VPD from Daymet V4 (Thornton et al., 2022) for the retained Ameriflux and NEON sites. We used GEE for the direct extraction of NLDAS-derived SW_IN and Daymet-derived VPD at a daily time step. Soil moisture and temperature were downloaded from the NASA Earthdata portal using the subset tools, then averaged to daily values in Google Colaboratory and stored in Google Cloud (Google Inc., CA, USA). The extracted environmental variable datasets were merged with STARFM fPAR every 5 days. Next, the merged dataset was joined with GPP measurements processed from Section 2.3. This resulting calibration dataset had more GPP data for the perennial and/or annual grass and grass-shrub mixture sites. Fewer data points were available for the grass-tree mixture and managed hay and pasture sites. In total, 24,239 GPP records (302 site-year combinations) were retained from 47 sites (SI: Table B2).

We carried out model calibration by adjusting vegetation type-based threshold values associated with the environmental modifiers, including maximum LUE as well as minimum and maximum root zone soil moisture, soil temperature, and VPD (SI: Fig. A2) based on GPP observations. The calibration was conducted using a Bayesian calibration scheme where initial values for model parameters were extracted from SMAP's L4C model (Endsley et al., 2020) for grasslands, and initial parameter ranges were obtained from literature review. The procedure was implemented using the BayesianTools package in R (Hartig et al., 2023). Three Markov chain

Monte Carlo (MCMC) chains were run in parallel for 5,000 iterations to obtain posterior distributions of model parameters with the assumption that the priors were weakly informative. Model convergence was examined using the scale reduction factor (Gelman & Rubin, 1989). The vegetation type-based model fits and results from leave-one-out cross-validation (LOOCV) for daily and cumulative (monthly, seasonal, and annual) GPP estimation were reported as Coefficient of Determination (R^2; Eq. 7), Root Mean Square Error (RMSE; Eq. 8), and Mean Bias Error (MBE; Eq. 9) for perennial and/or annual grass, grass-shrub mixture, and grass-tree mixture classes. For the managed hay and pasture class, evaluation was presented as model validation results using perennial and/or annual grass-specific parameters due to the limited number of available training sites within the managed hay and pasture class. The model calibration procedure was also carried out using MODIS fPAR inputs to enable a comparison with the use of STARFM inputs. Detailed model comparison results are presented in SI: Appendix C.

$$R^2 = 1 - \frac{\sum_{i=1}^{n}(y_i - \hat{y}_i)^2}{\sum_{i=1}^{n}(y_i - \bar{y})^2} \quad \text{(Eq. 7)}$$

$$RMSE = \sqrt{\frac{\sum_{i=1}^{n}(y_i - \hat{y}_i)^2}{n}} \quad \text{(Eq. 8)}$$

$$MBE = \frac{\sum_{i=1}^{n}(y_i - \hat{y}_i)}{n} \quad \text{(Eq. 9)}$$

Where n represents the number of samples, y_i represents observed value of sample i, $\hat{y}_i$ represents the model predicted value of sample i, and $\bar{y}$ represents the mean of observations.

2.6 Carbon model spin-up, calibration, and validation

The RCTM model adopts SMAP's L4C scheme (Endsley et al., 2020) by allocating GPP into net primary productivity (NPP) and autotrophic respiration. The NPP was then partitioned into aboveground and belowground biomass according to the vegetation type-specific root to shoot ratio. To account for the distribution of litter over time, we adopted DAYCENT's algorithms (Parton et al., 1998) to compute the amount of C transference from biomass pools into surface litter and dead roots for each time step. In this case, C flow is regulated by factors such as the day of the year and environmental modifiers including soil moisture and temperature. Subsequently, aboveground and belowground litter C were transferred into RCTM's SOM module that is adapted from RothC (Coleman & Jenkinson, 1996), which includes particulate organic C, humus organic C, and resistant organic C pools. The C flows among SOM pools are controlled by factors including soil texture, soil moisture, and soil temperature (SI: Fig. A3).

In RCTM, biomass and soil C pools were initialized by running the model for 2,000 years to reach an equilibrium that ensures the soil system is in equilibrium with the environmental conditions being simulated. The inputs for the spin-up were set to represent a "typical" condition for each site, for which we utilized STARFM fPAR, both surface 5 cm and root depth (ca. 60 cm) soil moisture, 5 cm soil temperature, and clay content from the 2002-2005 period. Soil moisture and temperature data were extracted from the NLDAS database (Xia et al., 2012), and clay content were obtained from the SoilGrid+ product (Ramcharan et al., 2018) (Table 1). Before conducting NEE calibration, we performed model spin-up for all retained Ameriflux and NEON sites using default model parameters obtained from SMAP's L4C, DAYCENT, and RothC models. GPP estimates, which are required for SOC calculation, were simulated using

vegetation type-specific, calibrated GPP parameters and inputs specified in Section 2.5. Both GPP and environmental variable datasets needed for model initialization were aggregated to a 5-day time step by averaging the results across all years. The goal was to obtain site-specific estimates of initial C pools to expedite the subsequent NEE calibration process.

The next step was to combine input datasets needed for NEE calibration with NEE measurements. The input data was generated at a five-day interval because of the STARFM output resolution. The combined dataset includes 22,820 NEE observations (364 site-year combinations) from 59 sites, while a larger number of observations were available for the perennial and/or annual grass and grass-shrub mixture sites compared to the grass-tree mixture or managed hay and pasture sites (SI: Table B2). We then carried out model calibration by optimizing vegetation type-specific parameters related to biomass partitioning, litterfall, and SOM decomposition (SI: Fig. A3) using NEE observations. In the calibration process, site-based estimates of initial C pools were used to spin up the model and then calculate C fluxes for 2002-2022. The calibration was implemented following the same procedure used for the GPP model (See Section 2.5). Again, model calibration was also implemented using MODIS fPAR inputs to enable a comparison with the use of STARFM inputs, which is presented in SI: Appendix C. Moreover, we presented model performance for estimating RECO in SI: Appendix D, where the absolute values of RECO fluxes were calculated as the difference between GPP and NEE.

After obtaining vegetation type-specific parameters through GPP and NEE calibrations, we ran RCTM for NEON sites to derive estimates of surface depth SOC stocks. Because the depth represented by RCTM cannot be clearly defined considering the various depths represented by model input layers, the results were compared against measurements of both 0-30 cm and 0-100 cm SOC stocks from 13 NEON sites as an evaluation of model performance for ranking the amount of SOC stocks in space.

2.7 Estimates of carbon fluxes for flux tower sites

The calibrated RCTM model was applied to all retained Ameriflux and NEON sites to derive estimates of GPP, NEE, and SOC stocks for a 20-year period (2003-2022). After averaging model outputs to annual results, the Pearson correlation was calculated in R between model input variables and RCTM outputs for site-year combinations. The purpose of this analysis was to explore climate and soil controls on the spatio-temporal dynamics in C fluxes. We aggregated and visualized model simulation results with regards to changes in SOC and C fluxes over time by vegetation types and geographic regions. Trend significance and slope of the time series data (GPP, NEE, and SOC) were calculated using a non-parametric Mann-Kendall test that detects monotonic upward or downward trends (Yue et al., 2002). The test was implemented in R with the ‘zyp’ package (Bronaugh et al., 2023) and applied to both individual Ameriflux/NEON sites and vegetation groups (SI: Appendix B). We also computed the correlation between site-based 20-year change in SOC stocks and climate, soil, and topographic variables (Table 1) to identify regional controlling factors for SOC sequestration in rangelands. Finally, a linear model for estimating SOC stock changes was determined through the application of a stepwise multiple linear regression (SMLR) approach in R using the Akaike Information Criterion (Bozdogan, 1987).

3 Results

3.1 Model accuracy for estimating rangeland productivity

The model performance associated with rangeland productivity prediction was evaluated using GPP modeling results. The performance of the calibration model for estimating daily GPP was the best for the grass-shrub mixture sites (R^2 = 0.70, RMSE = 0.9 g C m^{-2} day^{-1}), followed by the grass-tree mixture (R^2 = 0.60, RMSE = 1.1 g C m^{-2} day^{-1}) and perennial and/or annual grass sites (R^2 = 0.58, RMSE = 2.2 g C m^{-2} day^{-1}) (Fig. 3). The perennial and/or annual grass-specific model also obtained R^2 = 0.55 and RMSE = 3.3 g C m^{-2} day^{-1} for estimating daily GPP from the managed hay and pasture sites. Using LOOCV, RCTM was shown to have R^2 of approximately 0.60 for perennial and/or annual grass, grass-shrub mixture, and grass-tree mixture sites. The MBE values associated with the models revealed a slight underestimation of GPP using model outputs compared to flux tower measurements-derived estimates. This type of underestimation was the greatest for higher GPP observations.

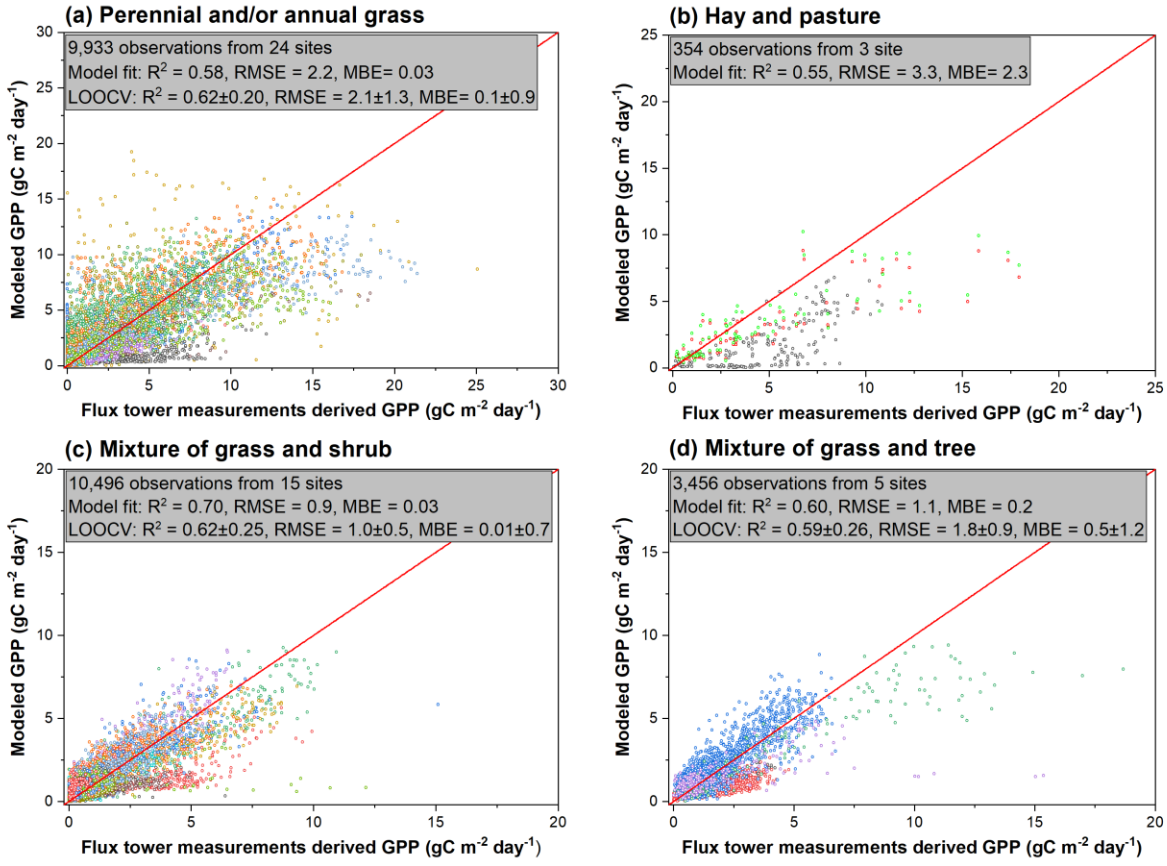

Figure 3. Gross primary productivity (GPP) model performance shown as coefficient of determination (R^2), root mean square error (RMSE, C m^{-2} day^{-1}), and mean bias error (MBE, C m^{-2} day^{-1}) for different vegetation classes including (a) perennial and/or annual grass, (b) managed hay and pasture, (c) mixture of grass and shrub, and (d) mixture of grass and tree classes. Both model fits and leave-one-out cross-validation (LOOCV) results are presented. Different colors represent different Ameriflux/NEON study sites.

Model performance for estimating rangeland productivity is strongly impacted by the seasons (Fig. 4a and c). During the growing season, model performance represented by R^2 was significantly higher (between 0.5 and 0.7) for all vegetation types compared to the winter season (Fig. 4a). The best model fit was achieved between June and August for perennial and/or annual grass and grass-tree mixture sites, while grass-shrub mixture sites had the best fit for March to May. However, it should be mentioned that the model RMSE was also noticeably higher during the growing season because winter GPP values were much lower in magnitude than those during the growing season. The results were similar among seasons for normalized RMSE values (Fig. 4c).

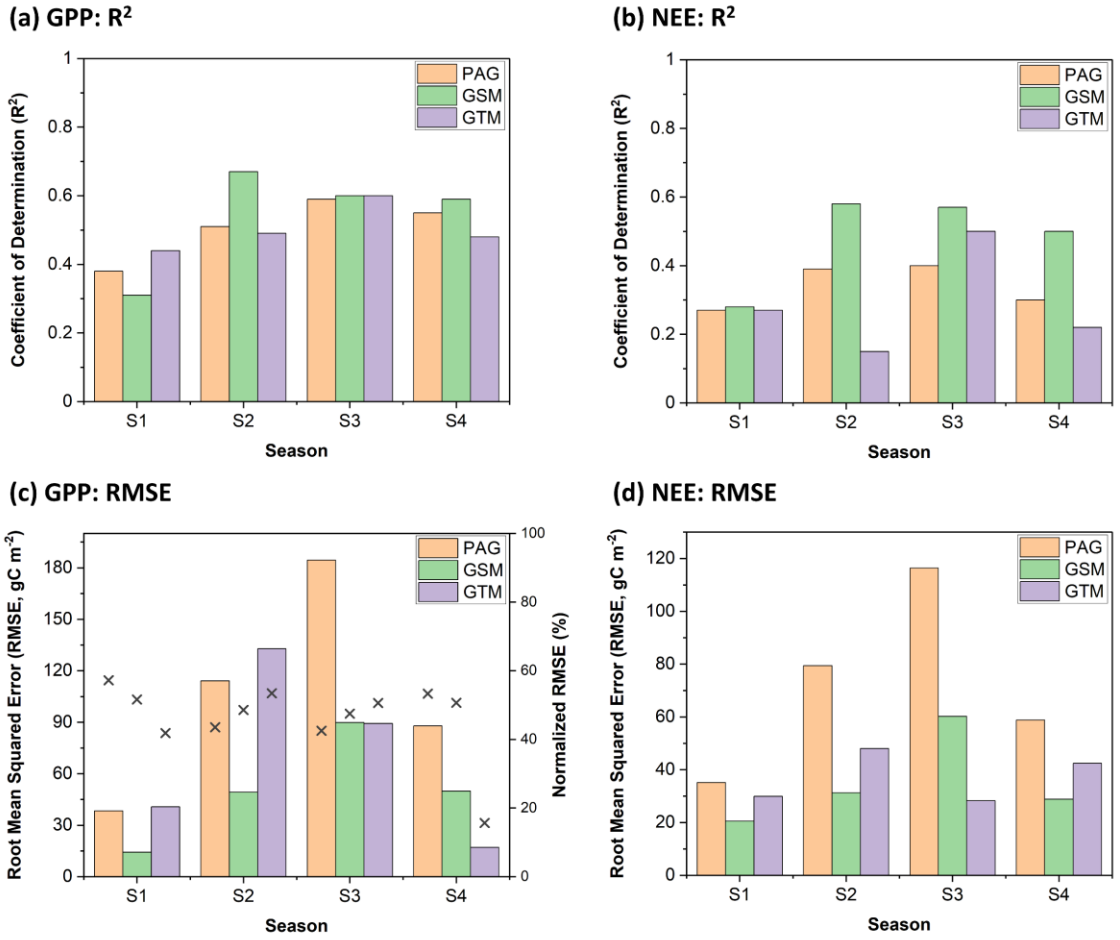

Figure 4. The model performance for estimating (a) gross primary productivity (GPP) represented by coefficient of determination (R^2), (b) net ecosystem exchange of CO_2 (NEE) represented by R^2, (c) GPP represented by root mean square error (RMSE, C m^{-2} per seasonal cumulative), and NEE represented by RMSE. The results are averaged from sites grouped by four seasons including S1 (Dec, Jan, Feb), S2 (Mar, Apr, May), S3 (Jun, Jul, Aug), and S4 (Sep, Oct, Nov). The model performance is presented for perennial and/or annual grass (PAG) sites, grass and shrub mixture (GSM) sites, and grass and tree mixture (GTM) sites. Normalized RMSE in (c) is denoted as cross mark (X), which is calculated as RMSE divided by mean GPP of the season.

The annual cumulative GPP estimates were more accurate for grass-shrub mixture (R^2 = 0.72, RMSE = 199 g C m^{-2} $year^{-1}$) than for the grass-tree mixture (R^2 = 0.68, RMSE = 387 g C m^{-2} $year^{-1}$) or perennial and/or annual grass (R^2 = 0.61, RMSE = 329 g C m^{-2} $year^{-1}$) sites (Table 2), which is consistent with model performance ranking for estimating daily GPP (Fig. 3). Despite the better model fit (R^2) in estimating daily GPP during the growing season, cumulative GPP estimates from April to October showed slightly lower accuracy compared to annual estimates, indicating that model bias might be reduced when integrating results from the growing and non-growing seasons. The model bias (MBE = 138 g C m^{-2} $year^{-1}$) was larger for the estimates of annual GPP for grass-tree mixture sites, showing a significant underestimation (Table 2). The model performance for estimating monthly cumulative GPP was similar among different vegetation types, with R^2 over 0.7. Again, model bias which indicates underestimation of GPP was higher for the grass-tree mixture sites.

Table 2. Model performance for estimating annual, seasonal, and monthly cumulative gross primary productivity (GPP) and net ecosystem exchange of CO_2 (NEE) shown as coefficient of determination (R^2), root mean square error (RMSE), and mean bias error (MBE) averaged from sites within different vegetation types. The growing season is set from April to October for comparison. Mean values are also calculated for different categories.

Vegetation class	GPP				NEE			
	Mean	R^2	RMSE	MBE	Mean	R^2	RMSE	MBE
Annual cumulative fluxes (g C m^{-2} $year^{-1}$)								
Perennial and/or annual grass	1096	0.61	329.1	15.9	105	0.40	180.0	103.7
Grass-shrub mixture	498	0.72	199.1	21.9	70	0.65	103.1	81.5
Grass-tree mixture	659	0.68	387.3	137.6	59	0.42	174.9	100.3
Growing season cumulative fluxes (g C m^{-2} per growing season)								
Perennial and/or annual grass	748	0.56	256.0	7.6	125	0.45	155.5	72.3
Grass-shrub mixture	352	0.72	146.5	18.7	84	0.69	93.6	68.0
Grass-tree mixture	432	0.64	187.6	16.6	41	0.40	120.7	50.6
Monthly cumulative fluxes (g C m^{-2} $month^{-1}$)								
Perennial and/or annual grass	79	0.72	49.8	2.0	9	0.42	34.2	8.6
Grass-shrub mixture	34	0.73	26.3	0.8	6	0.58	17.2	6.6
Grass-tree mixture	52	0.70	45.4	12.7	41	0.46	24.5	9.0

The model performance (R^2 between 0.6 and 0.7) for estimating cumulative annual or monthly RECO (SI: Table D1) was similar to that reported for GPP models (Table 2). Model estimates for RECO were more accurate for grass-shrub (R^2 = 0.64) or perennial and/or annual grass (R^2 = 0.60) sites compared to grass-tree (R^2 = 0.38) mixture sites (SI: Fig. D1).

3.2 Model accuracy for estimating net rangeland C fluxes and SOC stocks

The model performed better for estimating daily NEE from grass-shrub mixture (R^2 = 0.47, RMSE = 0.6 g C m^{-2} day^{-1}) and grass-tree mixture (R^2 = 0.37, RMSE = 0.8 g C m^{-2} day^{-1}) sites than the perennial and/or annual grass sites (R^2 = 0.27, RMSE = 1.6 g C m^{-2} day^{-1}) sites (Fig. 5). Daily NEE from the managed hay and pasture sites were estimated with limited accuracy using the perennial and/or annual grass -specific model (R^2 = 0.21, RMSE = 2.1 g C m^{-2} day^{-1}). The LOOCV results also suggest the need to further improve the NEE models, especially for the perennial and/or annual grass sites (R^2 = 0.32, MBE $\geq$ 0.3 g C m^{-2} day^{-1}).

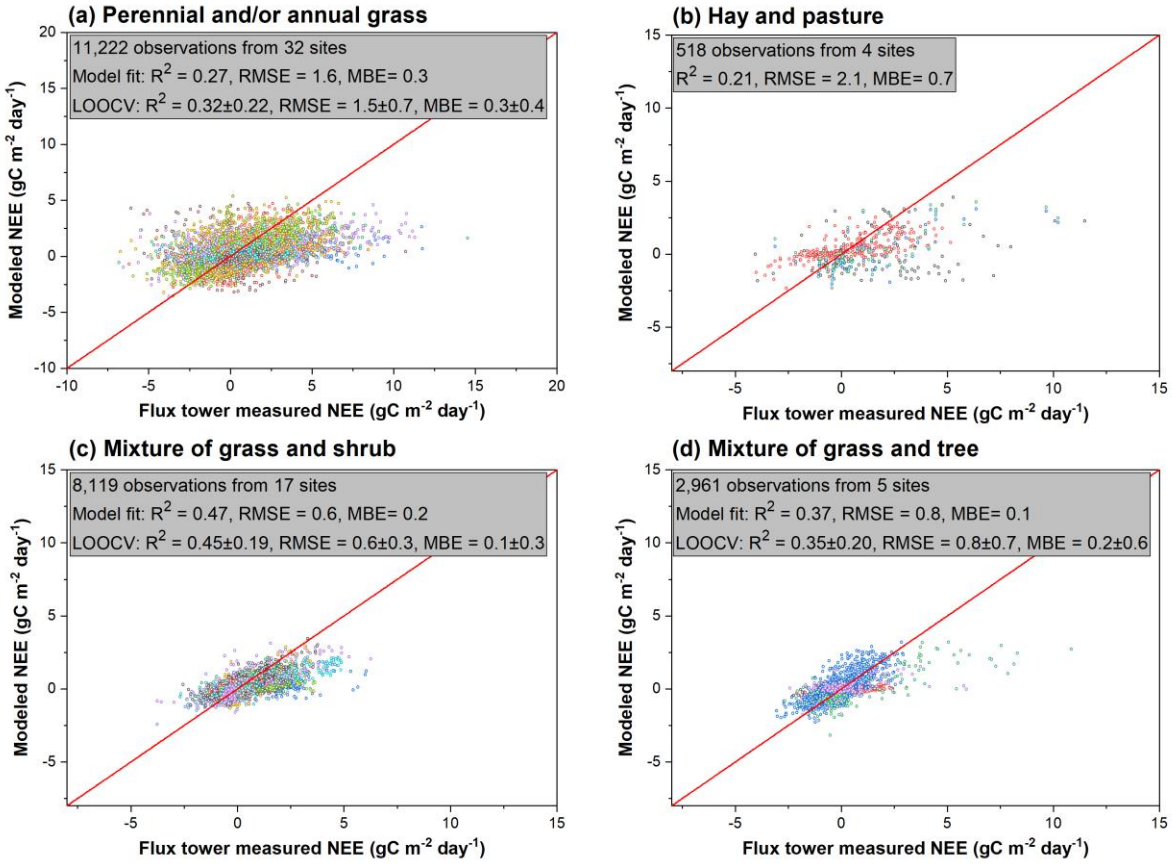

Figure 5. Net ecosystem exchange (NEE) model performance shown as coefficient of determination (R^2), root mean square error (RMSE, C m^{-2} day^{-1}), and mean bias error (MBE, C m^{-2} day^{-1}) for different vegetation classes including (a) perennial and/or annual grass, (b) managed hay and pasture, (c) mixture of grass and shrub, and (d) mixture of grass and tree classes. Positive NEE sign denotes ecosystem carbon sink activity. Both model fits and leave-one-out-cross-validation (LOOCV) results are presented. Different colors represent different Ameriflux/NEON study sites.

The model fit was also observed to be better for the growing season than for winter NEE estimates, with the exception of grass-tree mixture sites (Fig. 4b). Like GPP, model RMSE was higher for the growing season than for winter NEE (Fig. 4d). Even though the RCTM system showed limited success in estimating daily NEE flux (Fig. 5), the model performance was better for estimating monthly (R^2 between 0.4 and 0.6), growing season cumulative (R^2 between 0.4 and 0.7), or annual cumulative (R^2 between 0.4 and 0.7) NEE fluxes (Table 2). It is anticipated that the model performance was lower for NEE than for GPP or RECO considering that the model structure for estimating NEE is subject to uncertainty in simulating both grassland production and respiration, and that GPP and RECO might not have equivalent responses to climate conditions such as soil moisture and temperature (Table 3). Regardless of the temporal resolution (i.e., daily or cumulative) used for model performance evaluation, the RCTM performed consistently better for grass-shrub mixture sites.

The model-simulated surface SOC stocks agreed well with SOC measurements from NEON sites in terms of the ranking of the spatial dataset (R^2 = 0.58, Fig. 6). However, the model simulation results were higher than observed 0-30 cm SOC stocks (MBE = -2535 g m^{-2}). This is likely because RCTM inputs are not restricted to a specific depth layer (e.g., 30 cm) but are instead reflective of the integrated plant productivity signals due to the use of GPP and NEE data for model calibration. However, the RCTM simulated SOC stocks were significantly lower than those observed from the 0-100 cm depth (MBE = 7293 g m^{-2}, SI: Fig C3b), meaning that SOC stocks from 0-100 cm were too deep for RCTM to capture.

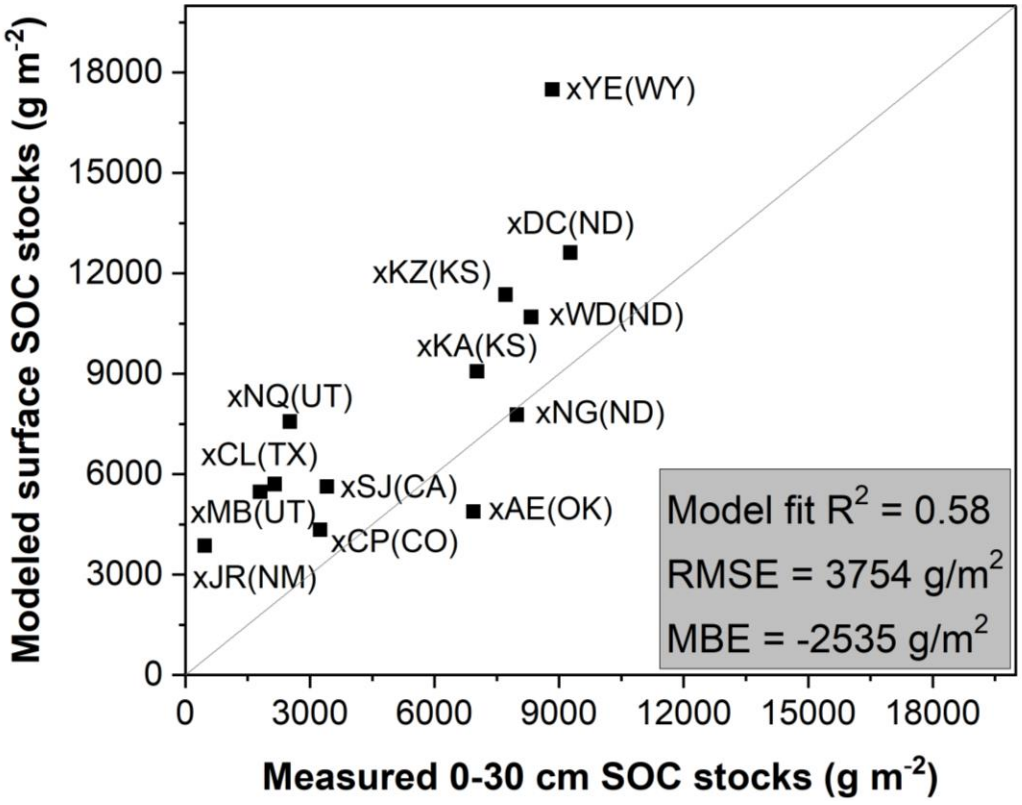

Figure 6. The model performance for estimating surface soil organic carbon (SOC) stocks for NEON grassland sites using calibrated Rangeland Carbon Tracking and Monitoring (RCTM) system.

3.3 Rangeland C dynamics influenced by site and environmental factors

The RCTM simulated annual cumulative GPP was strongly correlated with both surface (R = 0.7) and root zone soil moisture (R = 0.8), VPD (R = -0.4), and fPAR (R = 0.9) (Table 3). Strong correlations were observed between simulated annual average SOC and VPD (R = -0.4), soil temperature (R = -0.4), and fPAR (R = 0.6). The RCTM simulation also suggested significant correlations between RECO and all of the input variables investigated ($P < 0.05$). The annual cumulative NEE was less correlated with environmental variables used in the model (R < 0.2), which might be explained by the close to steady-state conditions of the sites. As expected, model-simulated SOC was significantly correlated with both GPP and RECO ($P < 0.05$).

Table 3. Correlation among model estimated annual cumulative net ecosystem exchange (NEE), gross primary productivity (GPP), ecosystem respiration (RECO), annual average soil organic carbon (SOC) stocks, and model input variables including 0-5 cm soil moisture (SWC_sf), root zone soil moisture (SWC_rt), vapor pressure deficit (VPD), 0-5 cm soil temperature (ST), clay content (Clay), and fraction of absorbed photosynthetically active radiation (fPAR).

	NEE	GPP	RECO	SOC	SWC_sf	SWC_rt	VPD	ST	Clay	fPAR
NEE	1									
GPP	0.26*	1								
RECO	0.15	0.99*	1							
SOC	-0.01*	0.41*	0.42*	1						
SWC_sf	0.14*	0.70*	0.19*	0.19*	1					
SWC_rt	0.15*	0.78*	0.25*	0.25*	0.97*	1				
VPD	-0.14*	-0.44*	-0.44*	-0.44*	-0.66*	-0.60*	1			
ST	-0.04	0.10*	-0.44*	-0.44*	-0.23*	-0.16*	0.71*	1		
Clay	0.01	0.09*	-0.01*	-0.01	0.10*	0.11*	0.09*	0.17*	1	
fPAR	0.20*	0.88*	0.56*	0.56*	0.62*	0.62*	-0.50*	-0.07*	-0.03	1

* The correlation is significant at $P < 0.05$.

The RCTM simulation was carried out to explore temporal patterns of C fluxes and SOC over the period from 2003 to 2022 influenced by vegetation types and geographic regions. It appears that both GPP and SOC stocks showed an increasing trend for Ameriflux and NEON sites grouped in perennial and/or annual grass, managed hay and pasture, and grass-shrub mixture classes (Fig. 7). According to model simulation results, surface SOC stocks increased by 4.7, 6.2, and 8.4 g C m^{-2} $year^{-1}$, for perennial and/or annual grass, managed hay and pasture, and grass-shrub mixture sites, respectively (SI: Appendix B). Similar trends in SOC sequestration were simulated for the majority of the USDA agricultural regions (Cooter et al., 2012), including Northern Great Plains (6.2 g C m^{-2} $year^{-1}$), Southern Great Plains (6.2 g C m^{-2} $year^{-1}$), Mountain regions (6.7 g C m^{-2} $year^{-1}$), and Midwest (10 g C m^{-2} $year^{-1}$), which are tied to an increase in GPP over time (SI: Fig. E1). For individual Ameriflux/NEON sites, RCTM simulated a significant ($P < 0.05$) increase trend in surface SOC stocks for the majority (69%) of the sites, with a smaller percentage (13%) associated with SOC decrease (SI: Table B3). While a GPP increase was simulated for 80% of the sites, the increase was found to be significant for only 16% of them. The most significant increases were found in Kellogg Biological Station sites in Michigan.

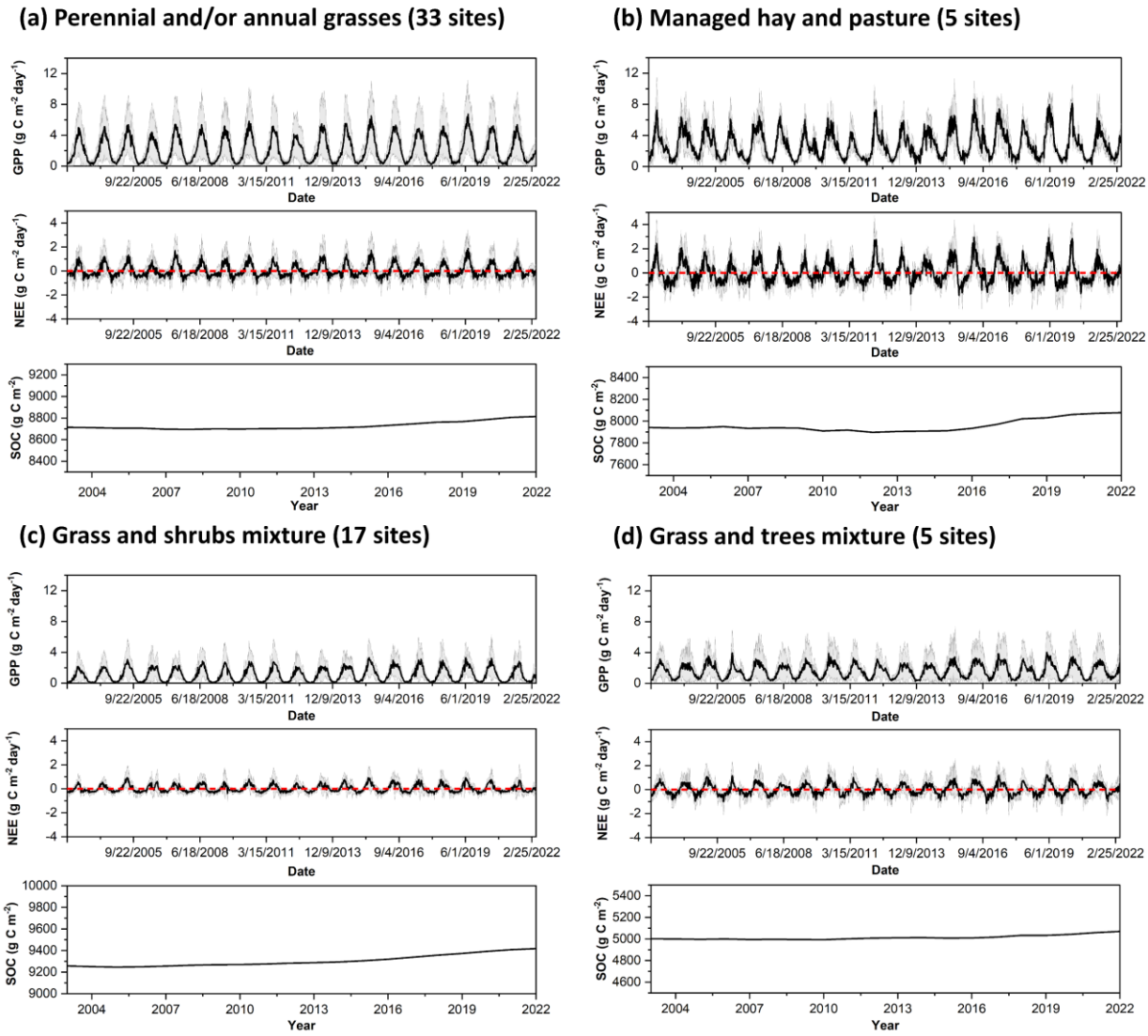

Figure 7. Model estimated temporal trends (2003-2022) in gross primary productivity (GPP), net ecosystem exchange (NEE), and surface soil organic carbon (SOC) stocks grouped by vegetation classes including (a) perennial and annual grass, (b) managed hay and pasture, (c) mixture of grass and shrub, and (d) mixture of grass and tree classes. The solid lines represent mean values averaged from all sites within the group, while the lighter-colored lines with areas filled within represent standard deviations for GPP and NEE estimates. The red line shows zero baseline for NEE where a positive NEE denotes ecosystem carbon sink activity. Different scales were used for SOC due to differences in data ranges among vegetation types.

4 Discussion

4.1 RCTM model performance compared to previous work

In comparison to previous research on estimating broad-scale rangeland productivity, our GPP model demonstrated similar or better performance. For example, Jin et al. (2020) carried

out a vegetation type-specific model calibration for the Mongolian Plateau, achieving a model performance of $R^2 = 0.57$ in estimating grassland NPP. Zhang et al. (2015) compared four LUE-type models with varying complexity and found less accurate model estimations for grasslands (R^2 between 0.45 and 0.64; RMSE between 1.9 and 2.6 g C m^{-2} day^{-1}) compared to croplands (R^2 between 0.59 and 0.73) using a global flux tower dataset. Also using a global flux tower dataset, Zhu et al. (2018) examined MODIS GPP products, which are also developed based on the LUE-type algorithms. Their study found moderate model fit ($R^2 = 0.66$) but relatively large RMSE, indicating an underestimation of grassland GPP. Work by Zhang et al. (2012) reported a model accuracy of $R^2 = 0.74$ for estimating annual GPP using the MODIS LUE algorithm when tested against an earlier flux tower dataset from U.S. grasslands. Calibrated against both Ameriflux and EuroFlux network sites, the work of Yuan et al. (2007) demonstrated better model performance than ours ($R^2 = 0.77$), likely because their dataset included not only grassland but also savanna and forest sites, allowing the LUE algorithms to better capture broader-scale climate and vegetation driving factors.

In contrast to the extensive modeling efforts dedicated to rangeland productivity estimation, there have been limited research efforts on modeling rangeland NEE and SOC, especially with the use of a RS-driven, process-based modeling approach like RCTM. We performed a comparison between RCTM and L4C (Endsley et al., 2020) using the Ameriflux/NEON sites (SI: Appendix F) and found that RCTM outperformed L4C results in terms of NEE estimates for perennial and/or annual grass and grass-shrub mixture sites, while the performance was similar for grass-tree mixture sites. This is not surprising because in the global L4C land-cover map, the single 'Grasslands' vegetation type (i.e., plant functional type) represents fairly different bioclimatic settings. The L4C parameters were calibrated using a global FLUXNET dataset that may not necessarily capture the interactions between climate factors and rangeland soil dynamics within a smaller region. Another explanation is that the STARFM fPAR inputs utilized by RCTM can better capture management-associated changes in rangeland C dynamics.

To compare our modeling results more broadly with rangeland modeling efforts, we identified several studies that focused on simulating regional-scale C dynamics using activity-driven process-based models. Abdalla et al. (2013) used the DNDC model to simulate C dynamics within Irish grasslands and reported a model performance for estimating monthly cumulative C fluxes ($R^2 = 0.51$) that is comparable to ours. The modeling work of Sándor et al. (2016) showed that both the biome-generic Biome-BGC ($R^2 = 0.28$) and the grassland-specific Pasture Simulation model ($R^2 = 0.42$) had limited model accuracy for estimating weekly NEE from European grassland sites, despite a higher model performance reported for GPP estimates ($R^2 > 0.75$). Limited accuracy was reported for simulating RECO from grassland sites using the CENTURY model, unless a time-lag factor is considered to account for legacy climate impacts (Kelly et al., 2000). Regarding SOC, Zhang et al. (2007) reported that CENTURY-simulated surface SOC stocks agreed well ($R^2 = 0.68$) with measurements at Qinghai-Tibetan Plateau sites. It should be noted that the variations in model performance between RCTM and these two studies can likely be attributed to differences in geographic coverage.

4.2 Factors driving regional rangeland C dynamics

The temporal trends observed for GPP and SOC changes are strongly controlled by the pattern observed in the RS-informed fPAR values. In perennial and/or annual grass, managed

hay and pasture, and grass-shrub mixture sites, GPP and SOC remained relatively constant until 2013 and then began to increase (Fig. 7). A similar trend was found for most of the regional-level summaries (SI: Fig. E1), which aligned with fPAR changes shown in SI: Appendix F. The fPAR values are often used to represent vegetation greenness (Forkel et al., 2014; Twine & Kucharik, 2008). In this context, rangeland greenness can be influenced both by environmental conditions and management practices (Browning et al., 2019; Long et al., 2019; Shibia et al., 2022).

The annual average fPAR correlated strongly ($R > 0.6$) with soil moisture (Table 3), which is in line with the significant correlations ($R > 0.5$, $P < 0.05$) computed between fPAR and annual precipitation at the regional scale (SI: Fig. G1). Our simulation results suggest that increased rangeland greenness was often associated with higher annual precipitation levels, particularly at the grass-shrub mixture and grass-tree mixture sites. This finding is in line with previous work that reported enhanced rangeland productivity in wetter years (Golodets et al., 2013; Liu et al., 2021; Scott et al., 2023). Strong correlation ($R = 0.64$) was also found between fPAR and air temperature for perennial and/or annual grass sites; however, this correlation was less certain for other vegetation types or aggregated at the regional scale (SI: Fig. G1). The uncertainty may stem from enhanced vegetation metabolism, increased SOM decomposition, and a prolonged growing season linked to higher temperatures, but is likely reversed by plant growth inhibition induced by heat or water stress (Izaurralde et al., 2011). In addition, vegetation composition (e.g., C3 versus C4) and ecoregion can often influence the magnitude and direction of climate effects on rangeland productivity and C dynamics (Fuhlendorf et al., 2000; Hossain & Li, 2021).

Conservation practices such as prescribed grazing management, grassland restoration, removal of invasive species, and upgrades of rangeland infrastructure can enhance rangeland greenness through the promotion of vegetation growth, increased biodiversity and resilience, reduced risks of wildfires, and improved water supply (Rolfe et al., 2021; Schmelzer et al., 2014; Silverman et al., 2019), while practices that lead to rangeland degradation can cause reduced rangeland greenness (Paudel & Andersen, 2010; Smet & Ward, 2005). Unfortunately, distinguishing management effects from climate variability on rangeland greenness can be challenging (Li et al., 2018), especially when there is a lack of detailed temporal information of grazing management (i.e., timing, intensity, and duration) and vegetation composition from most of the sites. Running RCTM at a 30 m spatial resolution would be useful to identify local areas of change in C dynamics, but ideally, assessing long-term changes in rangeland productivity and SOC from reference sites alongside sites undergoing practice changes can help identify management influence on rangeland C dynamics more effectively.

The simulation results showing a correlation between GPP and SOC stocks (Table 2) align with the expectation that productive rangeland can supply more C inputs to the soil. Elevated SOC levels were also explained by increased soil moisture at both depths, supporting the notion of higher rangeland productivity in response to higher moisture conditions. The negative correlation ($R = -0.44$, $P < 0.05$) between SOC and soil temperature likely reflects increased SOM decomposition tied to enhanced microbial activity in response to an increase in soil temperature (Hassan et al., 2015; Lal, 2004).

Environmental drivers are crucial not only for SOC stocks but also for changes in stock levels. Our SMLR analysis of RCTM outputs demonstrated that the rate of surface SOC stock changes was primarily controlled by site characteristics including slope, soil texture, air

temperature, and VPD (Eq. 10). The empirical SMLR model (R^2 = 0.58) developed on all retained Ameriflux and NEON sites suggested that rangeland SOC sequestration increased with clay content and air temperature but decreased with slope and VPD.

$$\Delta SOC = 818 - 35 \times \text{slope} + 6 \times \text{clay}(\%) + 50 \times \text{air temperature}(℃) - 114 \times \text{VPD}(\text{hPa}) \quad (\text{Eq. } 10)$$

Where ΔSOC $(g\ C\ m^{-2})$ denotes RCTM-simulated changes in surface SOC stocks from 2003 to 2022.

It is not surprising that soils with higher clay contents are connected to a higher SOC sequestration rate, because finer-textured soils can better protect SOM from decomposition through physical protection and chemical adsorption (Blanco-Canqui & Lal, 2004; Hassink, 1997). Likewise, studies have reported negative correlation between SOC accumulation and slope, which can be explained by enhanced biomass production tied to moisture and nutrient accumulation, as well as reduced erosion at lower-slope positions (Guillaume et al., 2021; Mensah et al., 2003). The higher SOC sequestration rate observed from warmer sites reflects increased rangeland productivity; however, temperature effects on SOC dynamics can be confounded by factors such as rangeland vegetation composition, soil texture, soil moisture, and grazing management practices (Bai & Cotrufo, 2022; Jones & Donnelly, 2004). Given that an increase in VPD indicates atmospheric drought, which is associated with soil moisture stress (Krishnan et al., 2012), it is anticipated that higher VPD values can lead to decreases in leaf conductance and assimilation rate and, subsequently, reduced grassland productivity and SOC sequestration rate (Shao et al., 2017; Zhang et al., 2023).

4.3 Limitations and future work

The discrepancy in modeled and measured SOC stocks points to the need to further refine RCTM to account for the diffusion and advection among different depth layers (Sanderman & Amundson, 2008; Yao Zhang et al., 2021) as well as the depth effects on SOC decomposition. The use of average environmental conditions from a relatively short period of time for model initialization, along with the fact that RS inputs might not fully capture management (e.g., irrigation) or legacy climate impacts on SOC dynamics (Delgado-Baquerizo et al., 2017; Nie et al., 2022), might also lead to estimation bias. It should be noted that RCTM or similar RS-driven process modeling approach-based systems are limited by the assumption that RS inputs can adequately capture management-driven (e.g., grazing, irrigation) changes in rangeland greenness. Future work should verify RCTM-simulated long-term trends in rangeland productivity with ground-truth biomass datasets. It would also be worthwhile to compare RCTM with activity-data driven models, such as DNDC (Li et al., 1994), DAYCENT (Parton et al., 1998), and MEMS (Robertson et al., 2019) to assess their accuracy and uncertainty in predicting the spatial and temporal C dynamics. Moreover, our modeling results found that RCTM had larger modeling bias for grass-tree mixture sites (Fig. 3), which might be associated with signal saturation in RS data caused by dense vegetation (Huete & Jackson, 1988; Zhu & Liu, 2015). The use of saturation or cloud-adjusted indices, as well as a combination of vegetation indices may be necessary to improve the accuracy of grass-tree mixture class-based modeling (Badgley et al., 2019; Gu et al., 2013; Yang et al., 2012). Also tied to RS inputs, the relatively lower model fit observed in the estimation of winter GPP and NEE (Fig. 4a and b) might be explained by the fact that the STARFM fusion method is constrained by a reduced number of Landsat and MODIS

images and pixels passing the QC criteria during the winter periods. This underscores the need to better account for snow cover effects and implement noise-reduction techniques in the case of missing data (Cao et al., 2018; Huang et al., 2021). Furthermore, the modeling bias for estimating NEE (Fig. 5) and SOC (Fig. 6) is significant, as reflected by the deviation of measured versus modeled values from the 1:1 line. This can lead to less accurate predictions, particularly at the lower and higher ends, pointing to the need for further model parameterization and evaluation using datasets covering a wider range.

There are several improvements that we believe can further increase the accuracy and applicability of RCTM. First, more accurate model input and parameter estimates, such as footprints calculated by Chu et al. (2021) and estimates of root:shoot ratio that are expressed as a function of climate factors (e.g., temperature, precipitation) and vegetation types (Hui & Jackson, 2006; Qi et al., 2019; Wang et al., 2021) for allocating modeled NPP into aboveground and belowground biomass, can be utilized. Parameterizing the RCTM for more detailed vegetation types such as annual versus perennial grass (Milne & Haynes, 2004), C3 versus C4 grass (Zhang et al., 2007), tallgrass versus shortgrass (Pepper et al., 2005), and pastures with different qualities (de Oliveira et al., 2022) that are known to have varying vegetation growth and C dynamics (Guerschman et al., 2003; Otunga et al., 2019; Wang et al., 2014) may help improve performance. Better capturing management (e.g., grazing and irrigation) effects on vegetation growth (Hao & He, 2019; Su et al., 2022), litter quality (Gao et al., 2020), and SOC dynamics (Conant et al., 2017; McSherry & Ritchie, 2013; Sanderson et al., 2020) may also improve the models performance and applicability to managed livestock operations. For example, the DNDC-type algorithms (Li et al., 2012) can be incorporated to better describe the conversion from animal ingested biomass into manure and the partition of manure into SOM pools. The model calibration and validation can be further strengthened by taking advantage of datasets reflecting long-term SOC stock changes associated with grassland management once such datasets become available through long-term monitoring networks (Chang et al., 2015; Moll-Mielewczik et al., 2023). Finally, the RCTM needs to be further evaluated for site-level estimates of rangeland productivity and C dynamics in order to inform management decisions by utilizing finer resolution data such as downscaled soil moisture datasets (Garcia-Cardona et al., 2022; Xia et al., 2022) as model inputs, and strategically selected local field samples for improved model calibration and validation.

5 Conclusions

The RCTM system is one of the first efforts to combine RS-driven LUE model outputs with a process-based soil model for the estimation of C dynamics and SOC stocks in rangeland systems. There is a potential to apply the system to estimate rangeland productivity and soil C dynamics for other regions of the world, after the system is calibrated and validated with datasets representing the application domain. The major advantages of RCTM include: (1) Applicability in situations where rangeland management datasets, such as grazing intensity and duration, are unavailable; (2) Capability to estimate long-term (20 years or more) rangeland C dynamics influenced by management and climate conditions; (3) Flexibility in the parameterization procedure which would allow continuous model improvement as new flux tower and SOC data become available; (4) Scalability in terms of its potential to be applied to different temporal scales and local or regional extents at relatively high spatial resolution (30 m) that would be relevant to management. The regional estimates of rangeland productivity and SOC sequestration

trends obtained from this work (e.g., increase in GPP and SOC tied to climate pattern) can be used to inform policy making and are suited to improve large scale rangeland C monitoring efforts, while it should also be possible to apply RCTM at the site level (individual operations) to improve management decisions, after parameterizing and verifying the system using site-level observations. High resolution, quality-controlled RS datasets and field observations capturing management effects on rangeland dynamics are essential to support the continuous improvement of RCTM and other RS-driven process-based modeling systems for rangeland C monitoring.

Acknowledgments

This research was supported by Conscience Bay Research, Woodwell Fund for Climate Solutions, Mighty Arrow Family Foundation, and J.M. Kaplan Fund. The authors extend their sincere gratitude to Ameriflux and NEON network PIs including Dr. Kimberly Novick, Dr. David Durden, Dr. Chris Florian, Dr. Cove Sturtevant, Dr. Stefan Metzger, Dr. David Bowling, Dr. Dennis Baldocchi, Dr. Camilo Rey-Sanchez, Dr. Sonia Wharton, Dr. Thomas Kolb, Dr. Sabina Dore, Dr. Dean Anderson, Dr. Elise Pendall, Dr. Mike Goulden, Dr. Roser Matamala, and Ross Bryant, for maintaining the sites and providing flux tower measurements. AmeriFlux is funded by the U.S. Department of Energy's Office of Science. Additional funding for a number of AmeriFlux sites in Arizona, New Mexico and Idaho comes from the U.S. Department of Agriculture's Long-term Agroecosystem Network. The National Ecological Observatory Network is a program sponsored by the National Science Foundation and operated under cooperative agreement by Battelle. The authors are also deeply grateful for the feedback and suggestions provided by Dr. Francesca Cotrufo for this project.

Open Research

The codes used to develop the Rangeland Carbon Tracking and Monitoring system in the study are made publicly available at Github: https://github.com/xiayushu/RCTM-soil-carbon.

References

Abdalla, M., Saunders, M., Hastings, A., Williams, M., Smith, P., Osborne, B., et al. (2013). Simulating the impacts of land use in Northwest Europe on Net Ecosystem Exchange (NEE): The role of arable ecosystems, grasslands and forest plantations in climate change mitigation. *Science of The Total Environment*, *465*, 325–336. https://doi.org/10.1016/j.scitotenv.2012.12.030

Ali, I., Cawkwell, F., Dwyer, E., Barrett, B., & Green, S. (2016). Satellite remote sensing of grasslands: From observation to management. *Journal of Plant Ecology*, *9*(6), 649–671. https://doi.org/10.1093/jpe/rtw005

Arndt, K. A., Campbell, E. E., Dorich, C. D., Grandy, A. S., Griffin, T. S., Ingraham, P., et al. (2022). Initial soil conditions outweigh management in a cool-season dairy farm's carbon sequestration potential. *Science of the Total Environment*, *809*, e152195. https://doi.org/10.1016/j.scitotenv.2021.152195

Badgley, G., Anderegg, L. D. L., Berry, J. A., & Field, C. B. (2019). Terrestrial gross primary production: Using NIR_V to scale from site to globe. *Global Change Biology*, *25*(11), 3731–3740. https://doi.org/10.1111/gcb.14729

Bai, Y., & Cotrufo, M. F. (2022). Grassland soil carbon sequestration: Current understanding, challenges, and solutions. *Science*, *377*(6606), 603–608. https://doi.org/10.1126/science.abo2380

Biederman, J. A., Scott, R. L., Bell, T. W., Bowling, D. R., Dore, S., Garatuza-Payan, J., et al. (2017). CO_2 exchange and evapotranspiration across dryland ecosystems of southwestern North America. *Global Change Biology*, *23*(10), 4204–4221. https://doi.org/10.1111/gcb.13686

Blanco-Canqui, H., & Lal, R. (2004). Mechanisms of Carbon Sequestration in Soil Aggregates. *Critical Reviews in Plant Sciences*, *23*(6), 481–504. Retrieved from https://doi.org/10.1080/07352680490886842

Booker, K., Huntsinger, L., Bartolome, J. W., Sayre, N. F., & Stewart, W. (2013). What can ecological science tell us about opportunities for carbon sequestration on arid rangelands in the United States? *Global Environmental Change*, *23*(1), 240–251. https://doi.org/10.1016/j.gloenvcha.2012.10.001

Bozdogan, H. (1987). Model selection and Akaike's Information Criterion (AIC): The general theory and its analytical extensions. *Psychometrika*, *52*(3), 345–370.

Bronaugh, D., Schoeneberg, A., & Zeman, L. (2023). Package'zyp.' Retrieved December 1, 2023, from https://cran.r-project.org/web/packages/zyp/zyp.pdf

Brown, T. B., Hultine, K. R., Steltzer, H., Denny, E. G., Denslow, M. W., Granados, J., et al. (2016). Using phenocams to monitor our changing earth: Toward a global phenocam network. *Frontiers in Ecology and the Environment*, *14*(2), 84–93. https://doi.org/10.1002/fee.1222

Browning, D. M., Snyder, K. A., & Herrick, J. E. (2019). Plant phenology: Taking the pulse of rangelands. *Rangelands*, *41*(3), 129–134. https://doi.org/10.1016/j.rala.2019.02.001

Cao, R., Chen, Y., Shen, M., Chen, J., Zhou, J., Wang, C., & Yang, W. (2018). A simple method to improve the quality of NDVI time-series data by integrating spatiotemporal information with the Savitzky-Golay filter. *Remote Sensing of Environment*, *217*, 244–257. https://doi.org/10.1016/j.rse.2018.08.022

Chang, X., Bao, X., Wang, S., Wilkes, A., Erdenetsetseg, B., Baival, B., et al. (2015). Simulating effects of grazing on soil organic carbon stocks in Mongolian grasslands. *Agriculture, Ecosystems & Environment*, *212*, 278–284. https://doi.org/10.1016/j.agee.2015.07.014

Chen, J., Chen, J., Liao, A., Cao, X., Chen, L., Chen, X., et al. (2015). Global land cover mapping at 30 m resolution: A POK-based operational approach. *ISPRS Journal of Photogrammetry and Remote Sensing*, *103*, 7–27. https://doi.org/10.1016/j.isprsjprs.2014.09.002

Chu, H., Luo, X., Ouyang, Z., Chan, W. S., Dengel, S., Biraud, S. C., et al. (2021). Representativeness of eddy-covariance flux footprints for areas surrounding AmeriFlux sites. *Agricultural and Forest Meteorology*, *301–302*, 108350. https://doi.org/10.1016/j.agrformet.2021.108350

Chu, H., Christianson, D. S., Cheah, Y. W., Pastorello, G., O'Brien, F., Geden, J., et al. (2023). AmeriFlux BASE data pipeline to support network growth and data sharing. *Scientific Data*, *10*(1), e614. https://doi.org/10.1038/s41597-023-02531-2

Coleman, K., & Jenkinson, D. S. (1996). RothC-26.3-A Model for the turnover of carbon in soil. In D. S. Powlson, P. Smith, & J. U. Smith (Eds.), *Evaluation of soil organic matter models: using existing long-term datasets* (pp. 237–246). Berlin, Germany: Springer. https://doi.org/https://doi.org/10.1007/978-3-642-61094-3_17

Conant, R. T., Cerri, C. E. P., Osborne, B. B., & Paustian, K. (2017). Grassland management impacts on soil carbon stocks: A new synthesis: A. *Ecological Applications*, *27*(2), 662–668. https://doi.org/10.1002/eap.1473

Cooter, E. J., Bash, J. O., Benson, V., & Ran, L. (2012). Linking agricultural crop management and air quality models for regional to national-scale nitrogen assessments. *Biogeosciences*, *9*(10), 4023–4035. https://doi.org/10.5194/bg-9-4023-2012

Delgado-Baquerizo, M., Eldridge, D. J., Maestre, F. T., Karunaratne, S. B., Trivedi, P., Reich, P. B., & Singh, B. K. (2017). Climate legacies drive global soil carbon stocks in terrestrial ecosystems. *Science Advances*, *3*(4), e1602008. https://doi.org/10.1126/sciadv.1602008

Derner, J. D., & Schuman, G. E. (2007). Carbon sequestration and rangelands: A synthesis of land management and precipitation effects. *Journal of Soil and Water Conservation*, *62*(2), 77–85. Retrieved from https://pubag.nal.usda.gov/download/10091/PDF

Derner, J. D., Augustine, D. J., & Frank, D. A. (2019). Does grazing matter for soil organic carbon sequestration in the western North American Great Plains? *Ecosystems*, *22*(5), 1088–1094. https://doi.org/10.1007/s10021-018-0324-3

Desai, A. R., Richardson, A. D., Moffat, A. M., Kattge, J., Hollinger, D. Y., Barr, A., et al. (2008). Cross-site evaluation of eddy covariance GPP and RE decomposition techniques. *Agricultural and Forest Meteorology*, *148*(6–7), 821–838. https://doi.org/10.1016/j.agrformet.2007.11.012

Doblas-Rodrigo, Á., Gallejones, P., Artetxe, A., Rosa, E., del Hierro, Ó., & Merino, P. (2022). Grassland contribution to soil organic carbon stock under climate change scenarios in Basque Country (Spain). *Regional Environmental Change*, *22*(1), 34. https://doi.org/10.1007/s10113-022-01877-4

Endsley, A. K., Kimball, J. S., Reichle, R. H., & Watts, J. D. (2020). Satellite monitoring of global surface soil organic carbon dynamics using the SMAP Level 4 carbon product. *Journal of Geophysical Research: Biogeosciences*, *125*(12), e2020JG006100. https://doi.org/10.1029/2020JG006100

Fargione, J. E., Boucher, T., Bridgham, S. D., Conant, R. T., Bassett, S., Cook-Patton, S. C., et al. (2018). Natural climate solutions for the United States. *Science Advances*, *4*(eeat1869), 1–14.

Forkel, M., Carvalhais, N., Schaphoff, S., Bloh, W. V., Migliavacca, M., Thurner, M., & Thonicke, K. (2014). Identifying environmental controls on vegetation greenness phenology through model-data integration. *Biogeosciences*, *11*(23), 7025–7050. https://doi.org/10.5194/bg-11-7025-2014

Fuhlendorf, S. D., Briske, D. D., & Smeins, F. E. (2000). Herbaceous vegetation change in variable rangeland environments: The relative contribution of grazing and climatic variability. *Applied Vegetation Science*, *4*(2), 177–188.

Gao, F., Masek, J., Schwaller, M., & Hall, F. (2006). On the blending of the landsat and MODIS surface reflectance: Predicting daily landsat surface reflectance. *IEEE Transactions on Geoscience and Remote Sensing*, *44*(8), 2207–2218. https://doi.org/10.1109/TGRS.2006.872081

Gao, J., Liang, T., Liu, J., Yin, J., Ge, J., Hou, M., et al. (2020). Potential of hyperspectral data and machine learning algorithms to estimate the forage carbon-nitrogen ratio in an alpine grassland ecosystem of the Tibetan Plateau. *ISPRS Journal of Photogrammetry and Remote Sensing*, *163*, 362–374. https://doi.org/10.1016/j.isprsjprs.2020.03.017

Garcia-Cardona, J., Ortega, A., & Rodriguez-Alvarez, N. (2022). Downscaling SMAP soil

moisture with Ecostress products using a graph-based interpolation method. *International Geoscience and Remote Sensing Symposium (IGARSS)*, *7*, 6169–6172. https://doi.org/10.1109/IGARSS46834.2022.9883945

Gelman, A., & Rubin, D. B. (1989). Inference from iterative simulation using multiple sequences. *Statistics*, *10*(1), 409–435. Retrieved from http://projecteuclid.org/euclid.ss/1177010123

Golodets, C., Sternberg, M., Kigel, J., Boeken, B., Henkin, Z., Seligman, N. G., & Ungar, E. D. (2013). From desert to Mediterranean rangelands: Will increasing drought and inter-annual rainfall variability affect herbaceous annual primary productivity? *Climatic Change*, *119*(3–4), 785–798. https://doi.org/10.1007/s10584-013-0758-8

Gorelick, N., Hancher, M., Dixon, M., Ilyushchenko, S., Thau, D., & Moore, R. (2017). Google Earth Engine: Planetary-scale geospatial analysis for everyone. *Remote Sensing of Environment*, *202*, 18–27. https://doi.org/10.1016/j.rse.2017.06.031

Gu, Y., Wylie, B. K., Howard, D. M., Phuyal, K. P., & Ji, L. (2013). NDVI saturation adjustment: A new approach for improving cropland performance estimates in the Greater Platte River Basin, USA. *Ecological Indicators*, *30*, 1–6. https://doi.org/10.1016/j.ecolind.2013.01.041

Guerschman, J. P., Paruelo, J. M., Di Bella, C., Giallorenzi, M. C., & Pacin, F. (2003). Land cover classification in the Argentine Pampas using multi-temporal Landsat TM data. *International Journal of Remote Sensing*, *24*(17), 3381–3402. https://doi.org/10.1080/0143116021000021288

Guillaume, T., Bragazza, L., Levasseur, C., Libohova, Z., & Sinaj, S. (2021). Long-term soil organic carbon dynamics in temperate cropland-grassland systems. *Agriculture, Ecosystems and Environment*, *305*, e107184. https://doi.org/10.1016/j.agee.2020.107184

Hall, D. K., Riggs, G. A., Salomonson, V. V., DiGirolamo, N. E., & Bayr, K. J. (2002). MODIS snow-cover products. *Remote Sensing of Environment*, *83*(1–2), 181–194. https://doi.org/10.1016/S0034-4257(02)00095-0

Hao, Y., & He, Z. (2019). Effects of grazing patterns on grassland biomass and soil environments in China: A meta-analysis. *PLoS ONE*, *14*(4), e0215223. https://doi.org/10.1371/journal.pone.0215223

Hartig, F., Minunno, F., Paul, S., Cameron, D., Tankred, O., & Maximilian, P. (2023). BayesianTools: General-purpose MCMC and SMC samplers and tools for bayesian statistics. Retrieved November 7, 2023, from https://cran.r-project.org/web/packages/BayesianTools/index.html

Hartigan, T., Hartigan, D. C., Maechler, M. M., Maechler, A. M., Ringach, D., Gpl, L., & Date, R. C. (2019). Package "tsoutliers": Detection of outliers in time series. Retrieved November 7, 2023, from http://r.meteo.uni.wroc.pl/web/packages/tsoutliers/tsoutliers.pdf

Hassan, W., Bano, R., Khatak, B. U., Hussain, I., Yousaf, M., & David, J. (2015). Temperature sensitivity and soil organic carbon pools decomposition under different moisture Regimes: EFFECT on total microbial and enzymatic activity. *Clean - Soil, Air, Water*, *43*(3), 391–398. https://doi.org/10.1002/clen.201300727

Hassink, J. (1997). The capacity of soils to preserve organic C and N by their association with clay and silt particles. *Plant and Soil*, *191*(1), 77–87. https://doi.org/10.1023/A:1004213929699

He, M., Chen, S., Lian, X., Wang, X., Peñuelas, J., & Piao, S. (2022). Global spectrum of vegetation light-use efficiency. *Geophysical Research Letters*, *49*(16), e2022GL099550.

https://doi.org/10.1029/2022GL099550
Heuvelink, G. B. M., Angelini, M. E., Poggio, L., Bai, Z., Batjes, N. H., van den Bosch, R., et al. (2021). Machine learning in space and time for modelling soil organic carbon change. *European Journal of Soil Science*, *72*(4), 1607–1623. https://doi.org/10.1111/ejss.12998
Hill, M. J., Roxburgh, S. H., McKeon, G. M., Carter, J. O., & Barrett, D. J. (2006). Analysis of soil carbon outcomes from interaction between climate and grazing pressure in Australian rangelands using Range-ASSESS. *Environmental Modelling and Software*, *21*(6), 779–801. https://doi.org/10.1016/j.envsoft.2005.02.006
Hinckley, E. L. S., Bonan, G. B., Bowen, G. J., Colman, B. P., Duffy, P. A., Goodale, C. L., et al. (2016). The soil and plant biogeochemistry sampling design for the National Ecological Observatory Network. *Ecosphere*, *7*(3), e01234. https://doi.org/10.1002/ecs2.1234
Holechek, J. L., Geli, H. M. E., Cibils, A. F., & Sawalhah, M. N. (2020). Climate change, rangelands, and sustainability of ranching in the Western United States. *Sustainability (Switzerland)*, *12*(12), e4942. https://doi.org/10.3390/su12124942
Homer, C., Dewitz, J., Fry, J., Coan, M., Hossain, N., Larson, C., et al. (2007). Completion of the 2001 National Land Cover Database for the counterminous United States. *Photogrammetric Engineering and Remote Sensing*, *73*(4), 337–341. Retrieved from http://www.ncbi.nlm.nih.gov/pmc/articles/PMC3339477/pdf/ehp.120-a152.pdf
Homer, C. G., Dewitz, J. A., Yang, L., Jin, S., Danielson, P., Xian, G., et al. (2015). Completion of the 2011 National Land Cover Database for the conterminous United States-Representing a decade of land cover change information. *Photogrammetric Engineering and Remote Sensing*, *81*(5), 345–354. https://doi.org/10.14358/PERS.81.5.345
Hossain, M. L., & Li, J. (2021). Biomass partitioning of C3- And C4-dominated grasslands in response to climatic variability and climate extremes. *Environmental Research Letters*, *16*(7), e074016. https://doi.org/10.1088/1748-9326/ac027a
Huang, K., Zhang, Y., Tagesson, T., Brandt, M., Wang, L., Chen, N., et al. (2021). The confounding effect of snow cover on assessing spring phenology from space: A new look at trends on the Tibetan Plateau. *Science of the Total Environment*, *756*, e144011. https://doi.org/10.1016/j.scitotenv.2020.144011
Huete, A. R., & Jackson, R. D. (1988). Soil and atmosphere influences on the spectra of partial canopies. *Remote Sensing of Environment*, *25*(1), 89–105. https://doi.org/10.1016/0034-4257(88)90043-0
Hui, D., & Jackson, R. B. (2006). Geographical and interannual variability in biomass partitioning in grassland ecosystems: A synthesis of field data. *New Phytologist*, *169*(1), 85–93. https://doi.org/10.1111/j.1469-8137.2005.01569.x
Izaurralde, R. C., Thomson, A. M., Morgan, J. A., Fay, P. A., Polley, H. W., & Hatfield, J. L. (2011). Climate impacts on agriculture: Implications for forage and rangeland production. *Agronomy Journal*, *103*(2), 371–381. https://doi.org/10.2134/agronj2010.0304
Jebari, A., Álvaro-Fuentes, J., Pardo, G., Almagro, M., & del Prado, A. (2021). Estimating soil organic carbon changes in managed temperate moist grasslands with RothC. *PLOS ONE*, *16*(8), e0256219. https://doi.org/10.1371/journal.pone.0256219
Jin, H., Bao, G., Chen, J., Chopping, M., Jin, E., Mandakh, U., et al. (2020). Modifying the maximal light-use efficiency for enhancing predictions of vegetation net primary productivity on the Mongolian Plateau. *International Journal of Remote Sensing*, *41*(10), 3740–3760. https://doi.org/10.1080/01431161.2019.1707902
Jones, M. B., & Donnelly, A. (2004). Carbon sequestration in temperate grassland ecosystems

and the influence of management, climate and elevated CO_2. *New Phytologist*, *164*(3), 423–439. https://doi.org/10.1111/j.1469-8137.2004.01201.x

Jones, M. O., Allred, B. W., Naugle, D. E., Maestas, J. D., Donnelly, P., Metz, L. J., et al. (2018). Innovation in rangeland monitoring: annual, 30 m, plant functional type percent cover maps for U.S. rangelands, 1984–2017. *Ecosphere*, *9*, e02430. https://doi.org/10.1002/ecs2.2430

Keller, M., Schimel, D. S., Hargrove, W. W., & Hoffman, F. M. (2008). A continental strategy for the National Ecological Observatory Network. *Frontiers in Ecology and the Environment*, *6*(5), 282–284. https://doi.org/10.1890/1540-9295(2008)6[282:ACSFTN]2.0.CO;2

Kelley, D. (2013). Package "oce": Analysis of oceanographic data. Retrieved November 7, 2023, from https://cran.r-project.org/web/packages/oce/oce.pdf

Kelly, R. H., Parton, W. J., Hartman, M. D., Stretch, L. K., Ojima, D. S., & Schimel, D. S. (2000). Intra-annual and interannual variability of ecosystem processes in shortgrass steppe. *Journal of Geophysical Research Atmospheres*, *105*(D15), 20093–20100. https://doi.org/10.1029/2000JD900259

Khalil, M. I., Fornara, D. A., & Osborne, B. (2020). Simulation and validation of long-term changes in soil organic carbon under permanent grassland using the DNDC model. *Geoderma*, *361*, 114014. https://doi.org/10.1016/j.geoderma.2019.114014

Kovalskyy, V., & Roy, D. P. (2013). The global availability of Landsat 5 TM and Landsat 7 ETM+ land surface observations and implications for global 30m Landsat data product generation. *Remote Sensing of Environment*, *130*, 280–293. https://doi.org/10.1016/j.rse.2012.12.003

Krause, A., Papastefanou, P., Gregor, K., Layritz, L. S., Zang, C. S., Buras, A., et al. (2022). Quantifying the impacts of land cover change on gross primary productivity globally. *Scientific Reports*, *12*(1), e18398. https://doi.org/10.1038/s41598-022-23120-0

Lal, R. (2004). Soil carbon sequestration to mitigate climate change. *Geoderma*, *123*(1–2), 1–22.

Lange, M., Feilhauer, H., Kühn, I., & Doktor, D. (2022). Mapping land-use intensity of grasslands in Germany with machine learning and Sentinel-2 time series. *Remote Sensing of Environment*, *277*, e112888. https://doi.org/10.1016/j.rse.2022.112888

Li, C., Frolking, S., & Harriss, R. (1994). Modeling carbon biogeochemistry in agricultural soils. *Global Biogeochemical Cycles*, *8*(3), 237–254. https://doi.org/10.1029/94GB00767

Li, C., Salas, W., Zhang, R., Krauter, C., Rotz, A., & Mitloehner, F. (2012). Manure-DNDC: A biogeochemical process model for quantifying greenhouse gas and ammonia emissions from livestock manure systems. *Nutrient Cycling in Agroecosystems*, *93*(2), 163–200. https://doi.org/10.1007/s10705-012-9507-z

Li, L., Zhang, Y., Liu, L., Wu, J., Li, S., Zhang, H., et al. (2018). Current challenges in distinguishing climatic and anthropogenic contributions to alpine grassland variation on the Tibetan Plateau. *Ecology and Evolution*, *8*(11), 5949–5963. https://doi.org/10.1002/ece3.4099

Liu, H., Jin, Y., Roche, L. M., O'Geen, A. T., & Dahlgren, R. A. (2021). Understanding spatial variability of forage production in California grasslands: Delineating climate, topography and soil controls. *Environmental Research Letters*, *16*(1), e014043. https://doi.org/10.1088/1748-9326/abc64d

Long, X., Guan, H., Sinclair, R., Batelaan, O., Facelli, J. M., Andrew, R. L., & Bestland, E. (2019). Response of vegetation cover to climate variability in protected and grazed arid

rangelands of South Australia. *Journal of Arid Environments*, *161*, 64–71. https://doi.org/10.1016/j.jaridenv.2018.10.001

Maher, A. T., Ashwell, N. E. Q., MacZko, K. A., Taylor, D. T., Tanaka, J. A., & Reeves, M. C. (2021). An economic valuation of federal and private grazing land ecosystem services supported by beef cattle ranching in the United States. *Translational Animal Science*, *5*(3), 1–15. https://doi.org/10.1093/tas/txab054

McSherry, M. E., & Ritchie, M. E. (2013). Effects of grazing on grassland soil carbon: A global review. *Global Change Biology*, *19*(5), 1347–1357. https://doi.org/10.1111/gcb.12144

Mensah, F., Schoenau, J. J., & Malhi, S. S. (2003). Soil carbon changes in cultivated and excavated land converted to grasses in east-central Saskatchewan. *Biogeochemistry*, *63*(1), 85–92. https://doi.org/10.1023/A:1023369500529

Milne, R. M., & Haynes, R. J. (2004). Soil organic matter, microbial properties, and aggregate stability under annual and perennial pastures. *Biology and Fertility of Soils*, *39*(3), 172–178. https://doi.org/10.1007/s00374-003-0698-y

Minasny, B., & McBratney, A. B. (2015). Digital soil mapping: A brief history and some lessons. *Geoderma*, *264*, 301–311. https://doi.org/10.1016/j.geoderma.2015.07.017

Moll-Mielewczik, J., Keel, S. G., & Gubler, A. (2023). Organic carbon contents of mineral grassland soils in Switzerland over the last 30 years. *Agriculture, Ecosystems and Environment*, *342*, e108258. https://doi.org/10.1016/j.agee.2022.108258

Nave, L. E., Bowman, M., Gallo, A., Hatten, J. A., Heckman, K. A., Matosziuk, L., et al. (2021). Patterns and predictors of soil organic carbon storage across a continental-scale network. *Biogeochemistry*, *156*(1), 75–96. https://doi.org/10.1007/s10533-020-00745-9

Nie, W., Kumar, S. V., Bindlish, R., Liu, P. W., & Wang, S. (2022). Remote sensing-based vegetation and soil moisture constraints reduce irrigation estimation uncertainty. *Environmental Research Letters*, *17*(8), e084010. https://doi.org/10.1088/1748-9326/ac7ed8

Novick, K. A., Biederman, J. A., Desai, A. R., Litvak, M. E., Moore, D. J. P., Scott, R. L., & Torn, M. S. (2018). The AmeriFlux network: A coalition of the willing. *Agricultural and Forest Meteorology*, *249*, 444–456. https://doi.org/10.1016/j.agrformet.2017.10.009

Numata, I., Roberts, D. A., Chadwick, O. A., Schimel, J., Sampaio, F. R., Leonidas, F. C., & Soares, J. V. (2007). Characterization of pasture biophysical properties and the impact of grazing intensity using remotely sensed data. *Remote Sensing of Environment*, *109*(3), 314–327. https://doi.org/10.1016/j.rse.2007.01.013

Oliphant, A. J. (2012). Terrestrial ecosystem-atmosphere exchange of CO_2, water and energy from FLUXNET: Review and meta-analysis of a global in-situ observatory. *Geography Compass*, *6*(12), 689–705. https://doi.org/10.1111/gec3.12009

de Oliveira, D. C., Maia, S. M. F., Freitas, R. de C. A., & Cerri, C. E. P. (2022). Changes in soil carbon and soil carbon sequestration potential under different types of pasture management in Brazil. *Regional Environmental Change*, *22*(3), e87. https://doi.org/10.1007/s10113-022-01945-9

Olson, D. M., Eric Dinerstein, Eric D. Wikramanayake, Neil D. Burgess, George V. N. Powell, Emma C. Underwood, et al. (2001). Terrestrial Ecoregions of the World: A New Map of Life on Earth. *BioScience*, *51*(11), 933–938.

Otunga, C., Odindi, J., Mutanga, O., & Adjorlolo, C. (2019). Evaluating the potential of the red edge channel for C3 (Festuca spp.) grass discrimination using Sentinel-2 and Rapid Eye satellite image data. *Geocarto International*, *34*(10), 1123–1143. https://doi.org/10.1080/10106049.2018.1474274

Parton, W. J., Hartman, M., Ojima, D., & Schimel, D. (1998). DAYCENT and its land surface submodel: Description and testing. *Global and Planetary Change*. Elsevier\. https://doi.org/10.1016/S0921-8181(98)00040-X

Paudel, K. P., & Andersen, P. (2010). Assessing rangeland degradation using multi temporal satellite images and grazing pressure surface model in Upper Mustang, Trans Himalaya, Nepal. *Remote Sensing of Environment*, *114*(8), 1845–1855. https://doi.org/10.1016/j.rse.2010.03.011

Pepper, D. A., Del Grosso, S. J., McMurtrie, R. E., & Parton, W. J. (2005). Simulated carbon sink response of shortgrass steppe, tallgrass prairie and forest ecosystems to rising [CO_2], temperature and nitrogen input. *Global Biogeochemical Cycles*, *19*(1), 1–20. https://doi.org/10.1029/2004GB002226

Phukubye, K., Mutema, M., Buthelezi, N., Muchaonyerwa, P., Cerri, C., & Chaplot, V. (2022). On the impact of grassland management on soil carbon stocks: a worldwide meta-analysis. *Geoderma Regional*, *28*, e00479. https://doi.org/10.1016/j.geodrs.2021.e00479

Qi, Y., Wei, W., Chen, C., & Chen, L. (2019). Plant root-shoot biomass allocation over diverse biomes: A global synthesis. *Global Ecology and Conservation*, *18*, e00606. https://doi.org/10.1016/j.gecco.2019.e00606

R Core Team. (2023). R: A language and environment for Statistical Computing. Retrieved April 12, 2023, from https://www.r-project.org/

Ramcharan, A., Hengl, T., Nauman, T., Brungard, C., Waltman, S., Wills, S., & Thompson, J. (2018). Soil property and class maps of the conterminous United States at 100-meter spatial resolution. *Soil Science Society of America Journal*, *82*(1), 186–201. https://doi.org/10.2136/sssaj2017.04.0122

Reeves, M. C., & Mitchell, J. E. (2011). Extent of coterminous US rangelands: Quantifying implications of differing agency perspectives. *Rangeland Ecology and Management*, *64*(6), 585–597. https://doi.org/10.2111/REM-D-11-00035.1

Reinermann, S., Asam, S., & Kuenzer, C. (2020). Remote sensing of grassland production and management-A review. *Remote Sensing*, *12*(12), e1949. https://doi.org/10.3390/rs12121949

Robertson, A. D., Paustian, K., Ogle, S., Wallenstein, M. D., Lugato, E., & Francesca Cotrufo, M. (2019). Unifying soil organic matter formation and persistence frameworks: The MEMS model. *Biogeosciences*, *16*(6), 1225–1248. https://doi.org/10.5194/bg-16-1225-2019

Rolfe, J., Star, M., & Curcio, A. (2021). Can extension programs improve grazing management in rangelands: A case study in Australia's Great Barrier Reef catchments. *Rangeland Journal*, *42*(6), 447–459. https://doi.org/10.1071/RJ20098

Rossum, G. Van, & Drake, F. L. (1995). *Python tutorial*. The Netherlands. Retrieved from http://www.python.org/doc/ref/

Roy, D. P., Wulder, M. A., Loveland, T. R., C.E., W., Allen, R. G., Anderson, M. C., et al. (2014). Landsat-8: Science and product vision for terrestrial global change research. *Remote Sensing of Environment*, *145*, 154–172. https://doi.org/10.1016/j.rse.2014.02.001

Sanderman, J., & Amundson, R. (2008). A comparative study of dissolved organic carbon transport and stabilization in California forest and grassland soils. *Biogeochemistry*, *89*(3), 309–327. https://doi.org/10.1007/s10533-008-9221-8

Sanderman, J., Hengl, T., & Fiske, G. J. (2017). Soil carbon debt of 12,000 years of human land use. *Proceedings of the National Academy of Sciences of the United States of America*, *114*(36), 9575–9580. https://doi.org/10.1073/pnas.1706103114

Sanderson, J. S., Beutler, C., Brown, J. R., Burke, I., Chapman, T., Conant, R. T., et al. (2020).

Cattle, conservation, and carbon in the western great plains. *Journal of Soil and Water Conservation*, *75*(1), 5A-12A. https://doi.org/10.2489/JSWC.75.1.5A

Sándor, R., Barcza, Z., Hidy, D., Lellei-Kovács, E., Ma, S., & Bellocchi, G. (2016). Modelling of grassland fluxes in Europe: Evaluation of two biogeochemical models. *Agriculture, Ecosystems and Environment*, *215*, 1–19. https://doi.org/10.1016/j.agee.2015.09.001

Santra, P., Kumar, M., Panwar, N. R., & Das, B. S. (2017). Digital soil mapping and best management of soil resources: A brief discussion with few case studies. In A. Rakshit, P. C. Abhilash, H. B. Singh, & S. Ghosh (Eds.), *Adaptive Soil Management: From Theory to Practices* (pp. 3–38). Singapore: Springer Singapore. https://doi.org/10.1007/978-981-10-3638-5_1

Schaaf, C., & Wang, Z. (2015). MODIS/Terra and Aqua Nadir BRDF-Adjusted Reflectance Daily L3 Global 500 m SIN Grid V006. https://doi.org/10.5067/MODIS/MCD43A4.061

Schmelzer, L., Perryman, B., Bruce, B., Schultz, B., McAdoo, K., McCuin, G., et al. (2014). CASE STUDY: Reducing cheatgrass (Bromus tectorum L.) fuel loads using fall cattle grazing. *Professional Animal Scientist*, *30*(2), 270–278. https://doi.org/10.15232/S1080-7446(15)30112-1

Scott, R. L., Johnston, M. R., Knowles, J. F., MacBean, N., Mahmud, K., Roby, M. C., & Dannenberg, M. P. (2023). Interannual variability of spring and summer monsoon growing season carbon exchange at a semiarid savanna over nearly two decades. *Agricultural and Forest Meteorology*, *339*, e109584. https://doi.org/10.1016/j.agrformet.2023.109584

Shao, C., Chen, J., Chu, H., Lafortezza, R., Dong, G., Abraha, M., et al. (2017). Grassland productivity and carbon sequestration in Mongolian grasslands: The underlying mechanisms and nomadic implications. *Environmental Research*, *159*, 124–134. https://doi.org/10.1016/j.envres.2017.08.001

Shibia, M. G., Röder, A., Fava, F. Pietro, Stellmes, M., & Hill, J. (2022). Integrating satellite images and topographic data for mapping seasonal grazing management units in pastoral landscapes of eastern Africa. *Journal of Arid Environments*, *197*, e104661. https://doi.org/10.1016/j.jaridenv.2021.104661

Sibanda, M., Mutanga, O., & Rouget, M. (2016). Comparing the spectral settings of the new generation broad and narrow band sensors in estimating biomass of native grasses grown under different management practices. *GIScience & Remote Sensing*, *53*(5), 614–633. https://doi.org/10.1080/15481603.2016.1221576

Silverman, N. L., Allred, B. W., Donnelly, J. P., Chapman, T. B., Maestas, J. D., Wheaton, J. M., et al. (2019). Low-tech riparian and wet meadow restoration increases vegetation productivity and resilience across semiarid rangelands. *Restoration Ecology*, *27*(2), 269–278. https://doi.org/10.1111/rec.12869

Smet, M., & Ward, D. (2005). A comparison of the effects of different rangeland management systems on plant species composition, diversity and vegetation structure in a semi-arid savanna. *African Journal of Range and Forage Science*, *22*(1), 59–71. https://doi.org/10.2989/10220110509485862

Smith, S. W., Vandenberghe, C., Hastings, A., Johnson, D., Pakeman, R. J., van der Wal, R., & Woodin, S. J. (2014). Optimizing carbon storage within a spatially heterogeneous upland grassland through sheep grazing management. *Ecosystems*, *17*(3), 418–429. https://doi.org/10.1007/s10021-013-9731-7

Stoy, P. C., Cook, A. A., Dore, J. E., Kljun, N., Kleindl, W., Jack Brookshire, E. N., & Gerken, T. (2021). Methane efflux from an American bison herd. *Biogeosciences*, *18*(3), 961–975.

https://doi.org/10.5194/bg-18-961-2021
Su, Y., Dong, K., Wang, C., & Liu, X. (2022). Grazing promoted plant litter decomposition and nutrient release: A meta-analysis. *Agriculture, Ecosystems and Environment*, *337*, e108051. https://doi.org/10.1016/j.agee.2022.108051
Sulman, B. N., Roman, D. T., Scanlon, T. M., Wang, L., & Novick, K. A. (2016). Comparing methods for partitioning a decade of carbon dioxide and water vapor fluxes in a temperate forest. *Agricultural and Forest Meteorology*, *226–227*, 229–245. https://doi.org/10.1016/j.agrformet.2016.06.002
Thornton, M. M., Thornton, P. E., Wei, Y., Mayer, B. W., Cook, R. B., & Vose, R. S. (2022). *Daymet: Monthly climate summaries on a 1-km grid for North America, version 4 R1*. *Oak Ridge National Laboratory*. Oak Ridge, Tennessee, USA. https://doi.org/10.3334/ORNLDAAC/2131
Tramontana, G., Migliavacca, M., Jung, M., Reichstein, M., Keenan, T. F., Camps-Valls, G., et al. (2020). Partitioning net carbon dioxide fluxes into photosynthesis and respiration using neural networks. *Global Change Biology*, *26*(9), 5235–5253. https://doi.org/10.1111/gcb.15203
Tucker, C. J. (1979). Red and photographic infrared linear combinations for monitoring vegetation. *Remote Sensing of Environment*. Elsevier\. https://doi.org/10.1016/0034-4257(79)90013-0
Turner, D. P., Ollinger, S. V., & Kimball, J. S. (2004). Integrating remote sensing and ecosystem process models for landscape- to regional-scale analysis of the carbon cycle. *BioScience*, *54*(6), 573–584. https://doi.org/10.1641/0006-3568(2004)054[0573:IRSAEP]2.0.CO;2
Twine, T. E., & Kucharik, C. J. (2008). Evaluating a terrestrial ecosystem model with satellite information of greenness. *Journal of Geophysical Research: Biogeosciences*, *113*(3), e2007JG000599. https://doi.org/10.1029/2007JG000599
United States Geological Survey. (2019). Phase 2 gap-fill algorithm: SLC-off gap-filled products gap-fill algorithm methodology. Retrieved October 1, 2023, from https://www.usgs.gov/media/files/landsat-7-slc-gap-filled-products-phase-two-methodology
Wang, C., Zhang, W., Li, X., Hou, Y., & Wu, J. (2021). A global meta-analysis of the effects of plant diversity on biomass partitioning in grasslands. *Environmental Research Letters*, *16*(6), e064083. https://doi.org/10.1088/1748-9326/ac0747
Wang, C., Zhong, C., & Yang, Z. (2014). Assessing bioenergy-driven agricultural land use change and biomass quantities in the U.S. Midwest with MODIS time series. *Journal of Applied Remote Sensing*, *8*(1), e085198. https://doi.org/10.1117/1.jrs.8.085198
Wang, G., Mao, J., Fan, L., Ma, X., & Li, Y. (2022). Effects of climate and grazing on the soil organic carbon dynamics of the grasslands in Northern Xinjiang during the past twenty years. *Global Ecology and Conservation*, *34*, e02039. https://doi.org/10.1016/j.gecco.2022.e02039
Wang, J., Liu, J., Cao, M., Liu, Y., Yu, G., Li, G., et al. (2011). Modelling carbon fluxes of different forests by coupling a remote-sensing model with an ecosystem process model. *International Journal of Remote Sensing*, *32*(21), 6539–6567. https://doi.org/10.1080/01431161.2010.512933
Waterhouse, H., Aburto, F., Rees, G., Griffin-LaHue, D. E., Salls, W. B., Rippner, D. A., et al. (2023). Diversified vegetation types on rangelands promote multiple soil-based ecosystem services. *Land Degradation & Development*. https://doi.org/10.1002/ldr.4967
Watts, J. D., Powell, S. L., Lawrence, R. L., & Hilker, T. (2011). Improved classification of

conservation tillage adoption using high temporal and synthetic satellite imagery. *Remote Sensing of Environment*, *115*(1), 66–75. https://doi.org/10.1016/j.rse.2010.08.005

Watts, J. D., Farina, M., Kimball, J. S., Schiferl, L. D., Liu, Z., Arndt, K. A., et al. (2023). Carbon uptake in Eurasian boreal forests dominates the high-latitude net ecosystem carbon budget. *Global Change Biology*, *29*(7), 1870–1889. https://doi.org/10.1111/gcb.16553

Williams, D. L., Goward, S., & Arvidson, T. (2006). Landsat: Yesterday, today, and tomorrow. *Photogrammetric Engineering and Remote Sensing*, *72*(10), 1171–1178. https://doi.org/10.14358/PERS.72.10.1171

Wilson, K. C., Rehmeier, R. L., Knight, G. L., Wiggam, S., Falke, J. A., Dalgleish, H. J., et al. (2008). Comparing ecosystem goods and services provided by restored and native lands. *BioScience*, *58*(9), 837–845. Retrieved from http://proxy.lib.sfu.ca/login?url=http://search.ebscohost.com/login.aspx?direct=true&db=eih&AN=34772285&site=ehost-live%0A10.1641/B580909

Xia, Y., Mitchell, K., Ek, M., Sheffield, J., Cosgrove, B., Wood, E., et al. (2012). NLDAS Noah Land Surface Model L4 Hourly 0.125 x 0.125 degree V002. Retrieved November 7, 2022, from https://disc.gsfc.nasa.gov/datasets/NLDAS_NOAH0125_H_002/summary

Xia, Y., Watts, J. D., Machmuller, M. B., & Sanderman, J. (2022). Machine learning based estimation of field-scale daily, high resolution, multi-depth soil moisture for the Western and Midwestern United States. *PeerJ*, *10*, e14275. https://doi.org/10.7717/peerj.14275

Xia, Y., Ford, T. W., Wu, Y., Quiring, S. M., & Ek, M. B. (2015). Automated quality control of in situ soil moisture from the North American Soil Moisture Database using NLDAS-2 products. *Journal of Applied Meteorology and Climatology*, *54*(6), 1267–1282. https://doi.org/10.1175/JAMC-D-14-0275.1

Xu, B., Yang, X. C., Tao, W. G., Qin, Z. H., Liu, H. Q., Miao, J. M., & Bi, Y. Y. (2008). Modis-based remote sensing monitoring of grass production in China. *International Journal of Remote Sensing*, *29*(17–18), 5313–5327. https://doi.org/10.1080/01431160802036276

Yagasaki, Y., & Shirato, Y. (2014). Assessment on the rates and potentials of soil organic carbon sequestration in agricultural lands in Japan using a process-based model and spatially explicit land-use change inventories – Part 2: Future potentials. *Biogeosciences*, *11*(16), 4443–4457. https://doi.org/10.5194/bg-11-4443-2014

Yang, J., Weisberg, P. J., & Bristow, N. A. (2012). Landsat remote sensing approaches for monitoring long-term tree cover dynamics in semi-arid woodlands: Comparison of vegetation indices and spectral mixture analysis. *Remote Sensing of Environment*, *119*, 62–71. https://doi.org/10.1016/j.rse.2011.12.004

Yuan, W., Liu, S., Zhou, G., Zhou, G., Tieszen, L. L., Baldocchi, D., et al. (2007). Deriving a light use efficiency model from eddy covariance flux data for predicting daily gross primary production across biomes. *Agricultural and Forest Meteorology*, *143*(3–4), 189–207. https://doi.org/10.1016/j.agrformet.2006.12.001

Yue, S., Pilon, P., Phinney, B., & Cavadias, G. (2002). The influence of autocorrelation on the ability to detect trend in hydrological series. *Hydrological Processes*, *16*(9), 1807–1829. https://doi.org/10.1002/hyp.1095

Zhang, F., Chen, J. M., Chen, J., Gough, C. M., Martin, T. A., & Dragoni, D. (2012). Evaluating spatial and temporal patterns of MODIS GPP over the conterminous U.S. against flux measurements and a process model. *Remote Sensing of Environment*, *124*, 717–729. https://doi.org/10.1016/j.rse.2012.06.023

Zhang, L., Wylie, B., Loveland, T., Fosnight, E., Tieszen, L. L., Ji, L., & Gilmanov, T. (2007).

Evaluation and comparison of gross primary production estimates for the Northern Great Plains grasslands. *Remote Sensing of Environment*, *106*(2), 173–189. https://doi.org/10.1016/j.rse.2006.08.012

Zhang, L. X., Zhou, D. C., Fan, J. W., & Hu, Z. M. (2015). Comparison of four light use efficiency models for estimating terrestrial gross primary production. *Ecological Modelling*, *300*, 30–39. https://doi.org/10.1016/j.ecolmodel.2015.01.001

Zhang, W., Zhang, F., Qi, J., & Hou, F. (2017). Modeling impacts of climate change and grazing effects on plant biomass and soil organic carbon in the Qinghai-Tibetan grasslands. *Biogeosciences*, *14*(23), 5455–5470. https://doi.org/10.5194/bg-14-5455-2017

Zhang, Y., Lavallee, J. M., Robertson, A. D., Even, R., Ogle, S. M., Paustian, K., & Cotrufo, M. F. (2021). Simulating measurable ecosystem carbon and nitrogen dynamics with the mechanistically defined MEMS 2.0 model. *Biogeosciences*, *18*(10), 3147–3171. https://doi.org/10.5194/bg-18-3147-2021

Zhang, Y., Tang, Y., Jiang, J., & Yang, Y. (2007). Characterizing the dynamics of soil organic carbon in grasslands on the Qinghai-Tibetan Plateau. *Science in China Series D: Earth Sciences*, *50*(1), 113–120. https://doi.org/10.1007/s11430-007-2032-2

Zhang, Z., Zhou, Y., Ju, W., Chen, J., & Xiao, J. (2023). Accumulated soil moisture deficit better indicates the effect of soil water stress on light use efficiency of grasslands during drought years. *Agricultural and Forest Meteorology*, *329*, e109276. https://doi.org/10.1016/j.agrformet.2022.109276

Zhou, W., Guan, K., Peng, B., Tang, J., Jin, Z., Jiang, C., et al. (2021). Quantifying carbon budget, crop yields and their responses to environmental variability using the ecosys model for U.S. Midwestern agroecosystems. *Agricultural and Forest Meteorology*, *307*, e108521. https://doi.org/10.1016/j.agrformet.2021.108521

Zhu, X., & Liu, D. (2015). Improving forest aboveground biomass estimation using seasonal Landsat NDVI time-series. *ISPRS Journal of Photogrammetry and Remote Sensing*, *102*, 222–231. https://doi.org/10.1016/j.isprsjprs.2014.08.014

Zhu, X., Pei, Y., Zheng, Z., Dong, J., Zhang, Y., Wang, J., et al. (2018). Underestimates of grassland gross primary production in MODIS standard products. *Remote Sensing*, *10*(11), e1771. https://doi.org/10.3390/rs10111771

van Zyl, J. J. (2001). The shuttle radar topography mission (SRTM): A breakthrough in remote sensing of topography. *Acta Astronautica*, *48*(5–12), 559–565. https://doi.org/10.1016/S0094-5765(01)00020-0